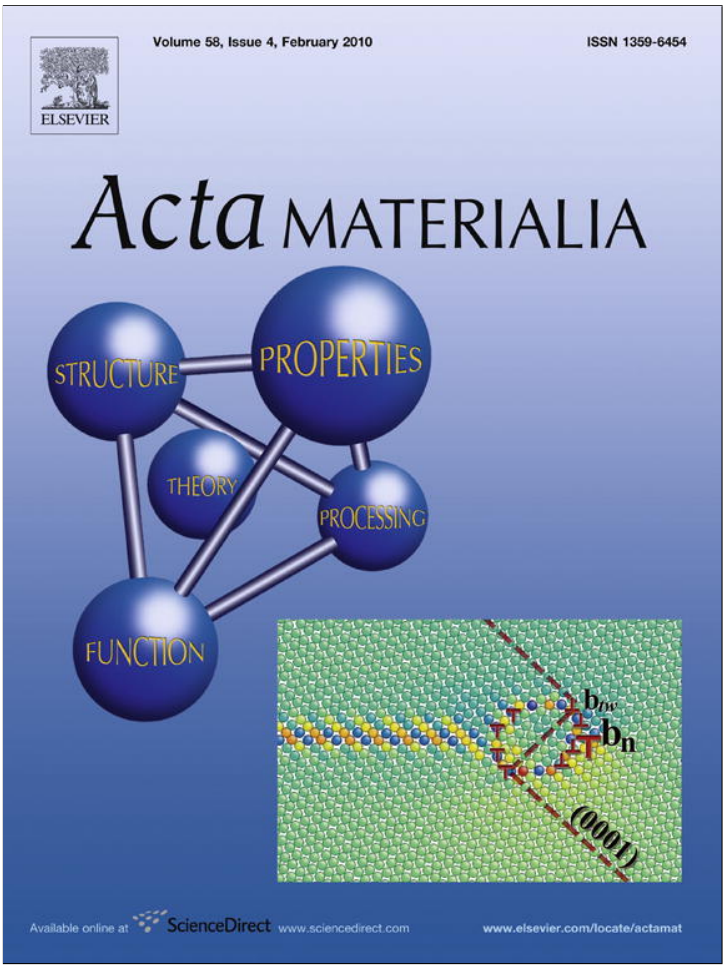

Available online at www.sciencedirect.com
ScienceDirect
Acta Materialia 58 (2010) 1212–1235
Acta MATERIALIA
www.elsevier.com/locate/actamat

Overview No. 150

Phase field modeling of defects and deformation

Yunzhi Wang [a,*], Ju Li [b]

[a] Department of Materials Science and Engineering, The Ohio State University, 2041 College Road, Columbus, OH 43210, USA
[b] Department of Materials Science and Engineering, University of Pennsylvania, 3231 Walnut Street, Philadelphia, PA 19104, USA

Received 16 April 2009; received in revised form 4 October 2009; accepted 24 October 2009
Available online 16 December 2009

Abstract

New perspectives on the phase field approach in modeling deformation and fracture at the fundamental defect level are reviewed. When applied at sub-angstrom length scales the phase field crystal (PFC) model is able to describe thermally averaged atomic configurations of defects and defect processes on diffusional timescales. When applied at individual defect levels the microscopic phase field (MPF) model is a superset of the Cahn–Hilliard description of chemical inhomogeneities and the Peierls (cohesive zone) description of displacive inhomogeneities. A unique feature associated with the MPF model is its ability to predict fundamental properties of individual defects such as size, formation energy, saddle point configuration and activation energy of defect nuclei, and the micromechanisms of their mutual interactions, directly using *ab initio* calculations as model inputs. When applied at the mesoscopic level the coarse grained phase field (CGPF) models have the ability to predict the evolution of microstructures consisting of a large assembly of both chemically and mechanically interacting defects through coupled displacive and diffusional mechanisms. It is noted that the purpose of the MPF model is fundamentally different from that of the CGPF models. The latter have been used primarily to study microstructural evolution with user-supplied linear response rate laws, defect energies and mobilities. Combined phase field simulations hold great promise in modeling deformation and fracture with complex microstructural and chemical interactions.

Keywords: Dislocation; Twinning; Martensitic transformation; Plasticity; Fracture

1. Introduction

Whether to use discrete particles or continuum fields to describe matter has been a long evolving theme in the development of science. Hooke's and Huygens' wave theory contrasted with Newton's particle theory of light until the establishment of quantum mechanics. In materials science using continuum fields to describe defects [1,2] and deformation [3] has been popular historically because it was analytically tractable. With the advent of computers continuum field approaches led naturally to numerical incarnations such as the finite element method [4]. On the other hand, computers also enabled discrete agent-based "computer experiments", such as atomistic simulations [5] of ensembles of atoms and kinetic Monte Carlo simulations of ensembles of defects. For instance, dislocation dynamics (DD) simulations [6–13] track the motion of many discrete dislocation segments to obtain information about dislocation organization and plasticity. When modeling materials behavior whether or not a field theoretic approach is advantageous compared with a discrete agent approach depends on the nature of the question asked and the lengthscale and timescale of interest. It is not always the case that the continuum approaches become less advantageous as the lengthscale shrinks. While discrete atom simulations are often appropriate to describe materials behavior in the tens of nanometers and nanoseconds range [14], if the lengthscale is further shrunk to the angstrom/sub-angstrom scale the continuum modeling approach becomes prevalent again, e.g. the density functional theory for electrons [15] is a continuum field theory. In contrast, the entire Earth was represented as a particle by Newton. For many problems an intimate coupling of

* Corresponding author. Tel.: +1 614 292 0682; fax: +1 614 292 1537.
E-mail address: wang.363@osu.edu (Y. Wang).

1359-6454/$36.00
doi:10.1016/j.actamat.2009.10.041

the field theoretic and discrete agent approaches is necessary [16–18]. For instance, DD simulations employ elementary continuum stress field solutions to treat dislocation segment–segment [19] and segment–boundary [20] interactions. The simulation results of DD may be better understood and used in the broader context when cast in the light of dislocation density-based continuum plasticity theory [21–37]. Atomistic simulations and continuum modeling may be seamlessly linked to solve problems in defects and deformation that would otherwise be difficult to solve [38–45].

In this overview we examine the development of a particular continuum field approach to modeling material defects and deformations, the phase field approach. The word "phase" in "phase field simulation" has its historical origin in "phase diagrams" and "phase transformations". Nowadays "phase" has, by consensus, a generalized meaning of order parameters, characterizing any chemical and structural non-uniformities such as chemical order, lattice orientation, inelastic strain, atomic density wave, etc. A modern view of inelastic deformation, i.e. a gross shape change of the material with finite free energy dissipation, is that it could be regarded as phase transition [46,47]. For example, shape memory and pseudoelasticity effects [48,49] involve large gross shape changes and obviously can be categorized as "deformation", but the underlying mechanism is martensitic transformation, a "phase transformation". Application of phase fields to modeling deformation therefore seems reasonable. The key defect carriers responsible for deformation, i.e. dislocations, have been modeled by the phase field method [50–57]. With the abilitiy to describe elastic inhomogeneity [58–63], surfaces [52,64–70] and voids [71–76], using phase fields to model fracture seems natural as well [70,74,77–89].

However, it is worth noting that historically the practice of phase field simulation grew largely out of modeling diffusional phase transformations [90–98], such as solidification and precipitation. Using the phase field method to model deformation is relatively recent, beginning with modeling of individual dislocations [50–57]. Rather than a weakness, we believe this historical development imparts strength to the phase field approach in modeling defects and deformation, especially in chemically and microstructurally complex materials. It gives impetus to the community to work towards developing a unified phase field methodology, under which one could treat displacive and diffusional degrees of freedom together in a seamless manner. Consider for instance dislocation–precipitate interactions in Ni-based superalloys [99,100]. On the one hand, the impedance of dislocation motion by intermetallic precipitates (precipitation hardening) is the dominant mechanism that imparts high strength to superalloys. Diffusive processes such as chemical reordering can couple strongly to dislocation shearing processes in governing the rate of deformation [101,102]. On the other hand, dislocation plasticity can also change the precipitate microstructure in the so-called rafting instability, where the precipitate morphologies change from an initial cuboidal shape to a plate or rod shape, which was recently modeled with the phase field approach [103–107]. These mechano-chemically or displacive-diffusionally coupled mechanisms, where microstructural evolution (e.g. grain growth [108–117], precipitate evolution [92,93,95,118–121], solute segregation [57,122–128]) blends in with mechanical deformation, would be quite difficult to model using a purely mechanical approach, and such deformation processes are by no means rare [129]. Because the phase field method is already well entrenched in modeling microstructural evolution with direct linkages to free energy and mobility databases [119,130–145], it appears that integrating deformation modeling into the same framework would be quite valuable.

Because of this historical context, and because the general phase field theory and its rapidly growing application in microstructural modeling on the mesoscale have been reviewed quite frequently in recent years [146–157], in this overview we address some new perspectives on the method in modeling deformation at individual defect levels, with a special emphasis on the treatment of the displacive degrees of freedom and coupled displacive–diffusional processes. The fundamentals of phase field methods for microstructure representation and the description of microstructure evolution at different length scales are first discussed in contrast to sharp interface models (Section 2). Then recent advances and quantitative aspects of microscopic phase field (MPF) models in predicting defect size and energy and thermally activated processes of defect nucleation, utilizing *ab initio* information such as generalized stacking fault (GSF) energy and multiplane generalized stacking fault (MGSF) energy as model inputs, are reviewed. In Section 3, the MPF model of dislocations is first compared quantitatively with the Peierls–Nabarro (PN) model and examples are presented to show its applications in the study of dislocation core structure and energy, Peierls stress and dislocation–precipitate interactions. Based on the kinship among dislocations, deformation twins, martensites and mode II and III cracks, the basic frameworks of using MPF models to study fundamental properties (including the saddle point configuration and activation energy) of these defects are discussed in the context of utilizing *ab initio* calculations of MGSF energy and transformation pathways as model inputs (Sections 4 and 5). Finally, phase field methods amenable to studies of coupled displacive–diffusional processes on both the nanometer (coarse grained phase field models) and sub-angstrom (i.e. phase field crystal models) length scales are reviewed and demonstrated (Sections 6 and 7). General concluding remarks are given in Section 8.

2. Fundamentals of the phase field method

2.1. Sharp interface and diffuse interface models

The collection of a hierarchy of structural and chemical non-uniformities (imperfections or defects) in solids consti-

tutes the so-called microstructure that in turn determines material properties. Well-known examples of these structural defects include dislocations, homophase and heterophase interfaces, surfaces, cracks and voids; while typical examples of chemical defects include concentration variations across heterophase interfaces and impurity segregation at various structural defects. Stacking faults, twin boundaries, anti-phase domain boundaries, grain boundaries and ferromagnetic and ferroelectric domain walls all belong to the category of homophase interfaces. In order to understand the mechanisms of microstructural evolution, the fundamental properties of these individual defects, which are the basic building blocks of a microstructure, have to be addressed.

There are two ways to treat chemical and structural non-uniformities associated with an interface in the thermodynamics of heterogeneous systems, i.e. the sharp interface model and diffuse interface model [158]. To avoid dealing with chemical and structural variations across an interface, which could be quite complex on the atomic scale [159], Gibbs formulated a simple phenomenological approach by introducing a hypothetical mathematical dividing surface [160,161]. The adjacent phases are assumed to be homogeneous right up to this dividing surface so that thermodynamics of homogeneous phases can be applied to each phase and various thermodynamic properties of the interface can be defined. In such a sharp interface model the interfacial width is zero and the interfacial energy is an input parameter rather than an output. Thus simulations based on the sharp interface model provide no insights into the nature of the interface. In contrast, the diffuse interface model assumes a continuous variation of composition, structure and other properties within the interfacial regions. It is based on the so-called gradient thermodynamics [162–164] where the total free energy of an arbitrary heterogeneous system is formulated as a function of both local chemical and structural states and their spatial variations (gradients). The gradient terms in the free energy appear naturally in a limit transition to the continuum of the discrete lattice models [165,166] and can be derived from microscopic theories in statistical mechanics [167,168], as well as from classical density functional theory [169]. Minimization of the total free energy determines the balances between the local free energy term, which prefers an infinitely sharp interface, and the gradient energy term, which prefers an infinitely wide interface and thus regularizes the interface width. In such a diffuse interface model, which lays the theoretical foundation for the phase field method, interfaces have finite equilibrium widths, unique chemical and structural variations within them and the associated interfacial energies. These fundamental properties of an interface are outputs of, rather than inputs to, the model.

Application of the diffuse interface model in predicting fundamental properties of extended defects was first demonstrated by Cahn and Hilliard, who studied the equilibrium concentration variation across a coherent interface, the width of the interface and the corresponding interfacial energy [164], and the concentration profile and activation energy of a critical nucleus [170]. As noted by Mullins [171] in his introduction to these two seminal papers, all these fundamental properties associated with an interface and a critical nucleus are expressed in terms of the parameters in the free energy model and there is no need to introduce the artificial dividing surface of Gibbs, nor to define a separate interfacial energy, nor to model the nucleus as homogeneous.

In parallel with the sharp interface and diffuse interface treatments of interfaces, there are two approaches to dislocation cores as well, i.e. the Volterra view [172] and the Peierls model [1]. In the Volterra view the defect is treated as a pure geometrical singularity in the continuum with zero core width. The core energy is rather an input than output of the model. In the Peierls model [1] the core has a finite width regularized by the interplay between two competing energy terms, the elastic energy term from materials outside the slipped region on the glide plane described by linear elasticity theory and the inelastic energy term from materials residing inside the slipped region (a one atomic layer thin plate) described by the generalized stacking fault (GSF) energy [173–176], a non-linear and oscillatory function with multiple minima. The elastic energy term (which depends on the gradient of the atomic displacement) prefers an infinitely wide dislocation core while the inelastic energy term (misfit energy, which depends on local displacement only) prefers the Volterra core. A compromise between the two yields the equilibrium core structure and the associated core energy. A similar model was developed for elastic relaxations in a misfitting epitaxial thin film on a rigid substrate [177], where the interplay between the misfit energy and the elastic energy determines the equilibrium non-uniform displacements in the film. Essentially the same treatment exists for inelastic tensile opening at the crack tip, called the cohesive zone model, where the crack tip stress solution is regularized by non-linear non-convex traction displacement laws of the separating material [178–186].

In the case of ferromagnetic and ferroelectric materials the crystalline anisotropy energy and Landau–Ginzburg–Devonshire free energy play the role of the misfit or crystalline energy; they depend on the local values of magnetization and polarization, respectively, and prefer infinitely sharp domain walls. The gradient energies depend on the magnetization and polarization gradients and prefer infinitely diffuse domain walls. The compromise between the two regularizes the domain wall thickness and determines the domain wall energy [152,163,187]. Of course, elastic, electrostatic and magnetostatic interactions at the domain walls also modify their structure and thickness.

These examples demonstrate that structural and chemical variations associated with an extended defect are regularized by force balance and tend to be diffuse at their natural length scales (i.e. nanometers). This is particularly true at the elevated temperatures where microstructural

evolution takes place. On these length scales the diffuse interface model has a unique advantage over the sharp interface model in predicting defect size, chemical and structural variation within the defect, the associated defect energy and defect nucleation and migration that have an activation lengthscale usually between 1 and 100 nm.

2.2. Phase fields

In a diffuse interface model the chemical and structural non-uniformities are characterized by two types of order parameters: conserved and non-conserved order parameters. Typical examples of the conserved order parameters include atomic density and concentration of a chemical species in a multi-component and/or multiphase system, while typical examples of the non-conserved order parameters include long-range order parameters for chemical ordering, magnetization and polarization for ferromagnetic and ferroelectric transitions and inelastic displacement or inelastic strain (eigenstrain or transformation strain) for dislocations, martensitic particles and microcracks. These order parameters are defined as continuous fields (functions of position) and are referred to as phase fields in phase field models. The total free energy of the system is formulated as a function of these fields. The variational derivatives of the free energy with respect to the fields drive their evolution over time following the generalized diffusion equation (Cahn–Hilliard equation [188]) for the conserved order parameters and the time-dependent Ginsburg–Landau equation [147] (also called the Allen–Cahn equation [189]) for the non-conserved order parameters. The discrete counterpart of the two equations is the microscopic diffusion equation [190], as shown in Wang [191]. The evolution over time of these order parameter fields completely define an evolving microstructure in a given materials system.

In order to take advantage of the unique ability of the diffuse interface model to predict fundamental properties of individual defects mentioned above it is essential to choose well-defined physical quantities as the order parameters in a phase field model. This seems to be straightforward in certain cases (such as the examples mentioned above), but could be quite challenging in some other cases, such as solidification and grain growth [151,192,193] where simple phenomenological order parameters were usually introduced to distinguish liquid from solid [151] and grains of one orientation from grains of other orientations [152]. Phase field models formulated with phenomenological order parameters are generally regarded as numerical techniques to avoid boundary tracking in describing evolving microstructures of complex geometries. It remains a challenge to define physically rigorous but computationally tractable order parameters in solidification and grain growth so a physical rather than phenomenological free energy model can be formulated and the fundamental properties of the solid–liquid interfaces and grain boundaries can be predicted using the phase field method. Recently, progress has been made in using amplitudes of atomic density functions as the physical order parameters to describe solidification and grain growth [169,194–196]. Alternatively, some of the order parameters introduced in atomistic simulations to identify these interfaces [197,198] could also be explored for such purposes.

2.3. Microscopic phase field model versus coarse grained phase field model

From the above discussions one should note that the diffuse interface model and phase field model were originally developed and used for the study of fundamental properties of extended defects, such as an interface [164] and a critical nucleus [170], whose size is comparable with the interfacial or core width. The model was subsequently applied to study spinodal decomposition [188] and spinodal ordering [189] where the entire system consists of interfaces at early stages. In all these applications the chemical or structural non-uniformities occur at length scales that are between 1 and 100 nm. At such length scales interfaces and dislocations tend to be diffuse naturally and the advantages of diffuse interface models over sharp interface models become obvious. In this overview phase field models being applied to individual defects at their natural length scales and hence being able to predict defect structure, chemistry, geometry and energy are referred to as microscopic phase field (MPF) models. In this regard, the original Cahn–Hilliard equation [164,170] and their discrete counterparts [165,199,200] are all MPF models. The newly developed MPF model of dislocations [56] and its relationship to the PN model will be discussed in Section 3, while MPF models of martensitic transformations [201,202] will be discussed in some detail in Section 4. As will be seen later, a unique advantage of the MPF models is their ability to directly incorporate *ab initio* calculations such as GSF energy [173–176] and MGSF energy [176,203–205] as their inputs to treat displacive processes (dislocations, martensitic transformations, cracks, etc.) and possible coupling with diffusional processes (e.g. interactions with solutes, precipitates and grain boundaries). The microscopic phase field model is much more efficient than full atomistic calculations, and more flexible, since it uses ab initio inputs directly and does not depend on the availability or accuracy of an interatomic potential [206]. The major assumption in the MPF model is that continuum theory is still applicable down to atomic length scales. The errors associated with such an assumption will be discussed in Section 3.

Over the past several decades phase field models on various coarse grained length scales have been developed to study collective behaviors of large microstructural ensembles such as dendritic solidification, grain growth and domain coarsening, dislocation network formation and coarsening and various phase transformations (for recent reviews see [70,149–157,207]). These coarse grained phase field (CGPF) models retain their advantages over the sharp

interface models in treating complicated geometrical and topological changes of defects during their microstructural evolution. Their applications have offered many valuable insights into the sequence of microstructural evolution and mechanisms of pattern formation in many materials systems during various materials processes. However, the interfacial thickness and dislocation core width resolved in the CGPF models far exceed their natural values and the models lose the intrinsic ability of a diffuse interface model to predict the fundamental properties of these defects. Moreover, CGPF models may provide quantitative rate information only in the so-called sharp interface limit [208], where the model parameters and additional terms in the equations governing the phase field are derived from the standard free boundary problem through sharp interface asymptotic analyses [151]. Such quantitative phase field simulations on the coarse grained level impose a serious constraint on the numerical grid density and, hence, computational efficiency. A new thin interface asymptotic analysis [208–212] has recently been developed to relax the restriction on the interface thickness. Some simple techniques [213,214] based on physical arguments of equivalent driving forces were also developed to increase the length scales of quantitative CGPF simulations. In the meantime, a multiphase field model [144,215] was proposed to completely decouple boundary width from boundary energy in the diffuse interface approach, so that the phase field method can be coarse grained to any arbitrary lengthscale without encountering unrealistically high interfacial energies. A thermodynamically consistent formulation of the model was derived by Kim et al. [216], now known as the KKS model. In addition, adaptive numerical algorithms [217–222] and new data structures [223,224] have also been developed to increase the computational efficiency of quantitative phase field simulations.

Although both MPF and CGPF models can be quantitative, the purpose of the MPF models is fundamentally different from that of the CGPF models. The CGPF models have been used to study microstructural evolution with linear response rate laws and user-supplied defect energy and mobility constants, while the MPF models have been used to calculate the equilibrium configurations of extended defects and their energies [54] using *ab initio* calculations as model inputs and to probe the total energy landscape using the nudged elastic band (NEB) technique, searching for saddle point configurations and activation energies of defect nuclei [202,225]. The outputs of MPF modeling serve as inputs of CGPF simulations.

3. Microscopic phase field model of dislocations

3.1. Field description of dislocations and order parameter

A dislocation in a crystal can be defined as the boundary between a slipped and an unslipped region or between two differently slipped regions (Fig. 1). The same description has been adopted in the phase field model of dislocations

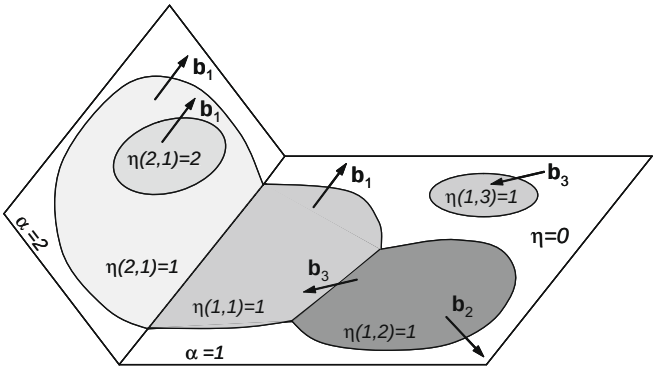

Fig. 1. Field representation of dislocations in the phase field method. The phase fields, $\eta(\alpha, m_\alpha)$, represent the amount of shear with respect to a perfect crystal in the unit b/d caused by sweeping of dislocations of $\mathbf{b}(\alpha, m_\alpha)$, where α and m_α represent the slip plane and slip direction, respectively, $\mathbf{b}$ is the Burgers vector and d is the interplanar distance of the glide planes.

[50], in which a slipped region is characterized by analogy to a martensitic platelet embedded in a parent phase matrix, with the thickness of the platelet being the interplanar spacing of the glide planes. In these cases the order parameters or phase fields describe inelastic strains of the defects, e.g. the transformation strain for a martensitic platelet and the eigenstrain for a dislocation loop enclosing the slipped region. In the latter the values of the phase fields, $\eta(\alpha, m_\alpha, \mathbf{r})$, represent the amount of inelastic shear with respect to a perfect crystal in the unit b/d at position $\mathbf{r}$ caused by sweeping of dislocations of $\mathbf{b}(\alpha, m_\alpha)$, where α and m_α represent the slip plane and slip direction, respectively, $\mathbf{b}$ is the Burgers vector and d is the interplanar distance of the glide planes. The spatial distribution of the inelastic strain associated with an arbitrary dislocation configuration consisting of dislocations from different slip systems can then be described through the phase fields as:

$$\varepsilon^0_{ij}(\mathbf{r}) = \sum_{\alpha, m_\alpha} \varepsilon^0_{ij}(\alpha, m_\alpha)\eta(\alpha, m_\alpha, \mathbf{r}) \tag{1}$$

where $\varepsilon^0_{ij}(\alpha, m_\alpha)$ is the eigenstrain of a dislocation loop. The phase fields, $\eta(\alpha, m_\alpha, \mathbf{r})$, serve as shape functions of the slipped regions.

3.2. Total energy functional and variational method

Starting from arbitrary values of the phase fields, $\eta(\alpha, m_\alpha, \mathbf{r})$, representing an arbitrary initial non-equilibrium microstructure, their equilibrium values or their evolutions towards equilibrium are obtained by total energy minimization. This is achieved by first formulating the total energy as a functional of the phase fields and then deriving the kinetics along the steepest descent path of the total energy using the time-dependent Ginsburg–Landau equation [147,189]. The total energy of a crystal with dislocations in the phase field model consists of three parts, the crystalline energy E^{cryst}, the elastic strain energy E^{elast} and the gradient energy E^{grad}, i.e.

$$E = E^{cryst} + E^{elast} + E^{grad} \tag{2}$$

The crystalline energy describes the potential energy in a crystal subjected to a general shear produced by arbitrary linear combinations of localized simple shears (slips) associated with all possible slip systems characterized by the phase fields, $\eta(\alpha, m_\alpha, \mathbf{r})$ [54]:

$$E^{cryst} = \int d\mathbf{r}\phi(\boldsymbol{\varepsilon}^0(\mathbf{r})) \tag{3}$$

where $\boldsymbol{\varepsilon}^0(\mathbf{r})$ is the general inelastic strain tensor given by Eq. (1). The crystalline energy is a periodic function reflecting the symmetry of the crystal. It replaces the Landau free energy in the phase field theory of martensitic transformations. For a particular slip plane the crystalline energy can be related [56] directly to the GSF energy (γ-surface) [173–176].

The elastic energy is associated with the elastic strains or elastic displacements of the crystal lattice caused by dislocations. In the microelasticity theory of Khachaturyan and Shatalov [226–228] (KS microelasticity theory hereafter), formulated on the framework of Eshelby [229,230], the elastic strain is expressed as the difference between the total strain and the inelastic strain. Then the elastic strain is relaxed instantaneously by minimizing the elastic energy with respect to the elastic displacement under a given inelastic strain through Green's function solution. This allows the elastic energy to be expressed as a function of the inelastic strain only in a closedform:

$$\begin{aligned} E^{el} = {} & \frac{1}{2}\sum_{\alpha,m_\alpha}\sum_{\beta,m_\beta}\fint B(\alpha,m_\alpha,\beta,m_\beta,\mathbf{g})\tilde{\eta}(\alpha,m_\alpha,\mathbf{g})\tilde{\eta}^*(\beta,m_\beta,\mathbf{g}) \\ & \times\frac{d\mathbf{g}}{(2\pi)^3} - \sigma_{ij}^{appl}\int\sum_{(\alpha,m_\alpha)}\varepsilon_{ij}^0(\alpha,m_\alpha)\eta(\alpha,m_\alpha,\mathbf{r})d\mathbf{r} \\ & - \frac{V}{2}S_{ijkl}\sigma_{ij}^{appl}\sigma_{kl}^{appl} \end{aligned} \tag{4}$$

where

$$\begin{aligned} B(\alpha,m_\alpha,\beta,m_\beta,\mathbf{g}) = {} & c_{ijkl}\varepsilon_{ij}^0(\alpha,m_\alpha)\varepsilon_{kl}^0(\beta,m_\beta) \\ & - n_i\sigma_{ij}^0(\alpha,m_\alpha)\Omega_{jk}(\mathbf{n})\sigma_{kl}^0(\beta,m_\beta)n_l \end{aligned}$$

C_{ijkl} is the elastic modulus tensor, $\sigma_{ij}^0 = C_{ijkl}\varepsilon_{kl}^0$, $\mathbf{g}$ is a vector in the reciprocal space and $\mathbf{n} = \mathbf{g}/g$, $[\Omega^{-1}(\mathbf{n})]_{ik} \equiv C_{ijkl}n_jn_l$ is the inverse of Green's function in the reciprocal space, $\tilde{\eta}(\mathbf{g})$ is the Fourier transform of $\eta(\mathbf{r})$ and $\tilde{\eta}^*(\mathbf{g})$ is the complex conjugate of $\tilde{\eta}(\mathbf{g})$. $\fint$ represents a principle value of the integral that excludes a small volume in the reciprocal space $(2\pi)^3/V$ at $\mathbf{g} = 0$, where V is the total volume of the system. S_{ijkl} is the elastic compliance tensor and σ_{ij}^{appl} is the applied stress.

The elastic energy in Eq. (4) is a closed form function of exactly the same variables (i.e. the phase fields) as for the crystalline energy. Then minimization of the total energy with respect to the inelastic strain fields (i.e. phase fields) is carried out numerically [231] by solving the time-dependent Ginzburg–Landau equations. It is therefore much more efficient than a full numerical minimization of the free energy with respect to the displacement because the Green's function solution eliminates the major part of the numerical minimization process.

According to gradient thermodynamics, the free energy of a heterogeneous system depends not only on local values of the order parameters but also on their special variations (i.e. gradients). Since structural non-uniformity (discontinuity) exists only within the core region of a dislocation, the gradient term has been formulated in such a way that it vanishes outside the core, i.e.

$$\begin{aligned} E^{grad} = \frac{1}{2}\int d\mathbf{r}\Bigg\{ & \sum_{\alpha,m_\alpha}\sum_{\beta,m_\beta}\xi(\alpha,m_\alpha,\beta,m_\beta)\frac{\mathbf{b}(\alpha,m_\alpha)\cdot\mathbf{b}(\beta,m_\beta)}{b(\alpha,m_\alpha)b(\alpha,m_\beta)} \\ & \times[\mathbf{n}(\alpha)\nabla\eta(\alpha,m_\alpha,\mathbf{r})]\cdot[\mathbf{n}(\beta)\times\nabla(\beta,m_\beta,\mathbf{r})]\Bigg\} \end{aligned} \tag{5}$$

where $\xi(\alpha, m_\alpha, \beta, m_\beta)$ is a parameter associated with the slip systems and $\mathbf{n}(\alpha)$ is the normal of the slip plane α. This form is obtained [54] from a general consideration of the total Burgers vector dependence of the line energy and thus produces results consistent with Frank's rule in cases of dislocation reactions, such as dislocation annihilation and dissociation.

Since the order parameter in the phase field model of dislocations is strain rather than displacement, which is proportional to the gradient of the displacement, the gradient energy actually accounts for contributions from high order derivatives of the displacement. It offers an independent degree of freedom to modify the Burgers vector distribution profile in the core region as compared with the PN model. As has been shown recently [56], the gradient energy term, although having little influence on the splitting distance of a dissociated core structure, affects the shapes (diffuseness) of the partial peaks. Furthermore, the gradient term is required for CGPF simulations of pattern formation associated with dislocation–dislocation and dislocation–precipitate interactions over length scales much coarser than the dislocation core size. It allows the generation of 'numerically' smooth core profiles on such length scales (e.g. several grid sizes wide, irrespective of the actual grid size) to ensure a mesh-independent evolution kinetics.

Through Eqs. (3)–(5) all the energy terms become sole functionals of the phase fields, $\eta(\alpha, m_\alpha, \mathbf{r})$. It is thus possible to compute the total driving forces as a combination of the crystalline, elastic and gradient energy

$$\frac{\delta(E^{cryst} + E^{elast} + E^{grad})}{\delta\eta(\alpha,m_\alpha,\mathbf{r})} \tag{6}$$

which are the variational derivatives of the total energy with respect to the same set of phase fields $\eta(\alpha, m_\alpha, \mathbf{r})$.

3.3. Comparison with the PN model

3.3.1. Similarities

Even though the phase field method for dislocations was first introduced [50] in the context of analogy to phase field

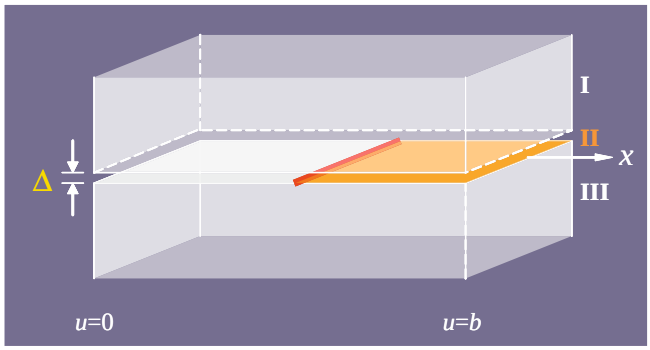

Fig. 2. Peierls partition of a crystal containing a dislocation. Regions I and III are assumed to be pure elastic while region II is treated as a non-Hookean slab having a thickness Δ which is the d spacing of the glide planes. u is the displacement.

descriptions of martensitic transformations, it is essentially a three-dimensional generalization of the PN model [1,232]. In the Peierls picture of a crystal containing a dislocation (Fig. 2) the total energy of the system is assumed to be composed of two parts, an elastic energy term that comes from the strain energy of materials outside the one atomic layer slip plane region (region II in Fig. 2) (referred to as the non-Hookean slab [233] or shear shocks [14]) and is described by linear elasticity theory, and a misfit energy term residing inside the non-Hookean slab and is described by the GSF potential. Even though not specified in the PN model, the non-Hookean slab should have a thickness equal to the interplanar distance of the glide planes, since it was implied in the formulation of the misfit energy. In the phase field model such a partition is realized automatically through the phase field description of a dislocation, e.g. $\eta(\alpha, m_\alpha, \mathbf{r})$ vanishes outside the non-Hookean slab.

Rather than a purely mathematical scheme, the partition of the two energy terms and regularization of defect cores in the Peierls model and the phase field model are physically inspired, and asymptotically exact within the limits of wide cores due to the short-range nature of interatomic potential. There are indeed two kinds of atoms in a crystal containing dislocations created by shear: those which are displaced so much that they change neighbors and those which are displaced but not enough to alter the local neighboring order. The first kind of relative displacement is non-perturbative and irreversible – it is the microscopic carrier of inelastic strain, which is localized in the sheared regions [14] – and the resulting energy (misfit or crystalline energy) can only be described by GSF energy, a non-linear and oscillatory function with multiple minima. The second kind of relative displacement is reversible (still in the same local potential energy basin as before) and a perturbative treatment such as linear elasticity may give some, but not catastrophic error, in modeling the elastic energy. The two energy terms compete in the total energy: the elastic energy prefers an infinitely wide dislocation core, but the misfit energy prefers a Volterra core, so the compromise is a finite core width in the continuum [1,232,234–236].

In the phase field model both the crystalline energy and the elastic energy are formulated in three-dimensions. For example, the crystalline energy in the phase field model describes the periodic potential of a crystal with respect to a general inelastic strain produced by arbitrary linear combinations of localized simple shears (slips) associated with all possible slip systems in a crystal [50,54]. It reduces to the GSF energy (γ-surface) when projected onto a particular slip plane. The KS microelasticity formulation [227,228] is a superset of the Peierls model. The total elastic energy $E[\eta(\alpha, m_\alpha, \mathbf{r})]$ is based on linear elasticity and implemented using the exact three-dimensional continuum Green's function to describe the long-range elastic interaction between $\nabla\eta(\alpha, m_\alpha, \mathbf{r})$ volume elements [95,118,228,237]. The volume element to volume element interaction kernel of $1/r$ type is more general than what has been employed in past Peierls–Nabarro type models [1,232,234–236,238–241] for dislocations, which used a dislocation density [in essence $\nabla\eta(\alpha, m_\alpha, \mathbf{r})$] infinite ribbon to infinite ribbon interaction kernel of $\log(r)$ type. In the degenerate case of straight dislocations these two integrals give exactly the same elastic energy. Yet when the symmetry is broken in the dislocation line direction, the $\log(r)$ kernel is no longer applicable, but the phase field energy function continues to work, as demonstrated [50,56]. In addition, elastic anisotropy is accounted for naturally in the phase field model [228]. Recently the phase field model has been extended to handle moduli inhomogeneities [62,63,242], such as cracks and voids [70,73–76,79,81,83,89], making it even more versatile. Because of the field description of defects, the complexity of computation is independent of the complexity of the defect configurations and morphologies. Essentially, the treatment is identical for defects of arbitrary types, shapes and spatial distributions (e.g. straight or curved, co-planar or non-co-planar dislocations). The phase field numerical machinery based on fast Fourier transformation (FFT) on real and reciprocal space regular grids gives this method outstanding numerical efficiency and stability, similar to planewave density functional theory (DFT) codes [243].

3.3.2. Differences

Nevertheless, there are several significant differences between the phase field and the PN models [56]. For example, gradient terms are introduced in the phase field model based on the gradient thermodynamics, which are absent in the PN model. In the elastic energy calculation the volume of the non-Hookean slab is excluded in the PN model, while it is included in the conventional phase field model. Burgers vector distribution in the PN model is confined within the non-Hookean slab, while the conventional phase field model does not impose such a constraint and inelastic strain relaxation is allowed outside the slip plane. Below we address these differences in some detail.

3.3.2.1. Role of the gradient term. The physical origin of the gradient energy term is associated with changes in atomic bonding from one location to neighboring locations. As

mentioned earlier, the gradient term appears naturally in a limit transition to the continuum of the discrete counterparts [165,166] of the gradient thermodynamics and can be derived from microscopic theories of statistical mechanics (see, for example, [167,168]) and from classical density function theory [169]. By comparing the continuum model against its discrete counterpart, Lee and Aaronson [166] showed that the interfacial energy predicted by the Cahn–Hilliard model [164] starts to deviate from the discrete model at low temperatures where the interfacial energy becomes anisotropic [e.g. (1 1 1), (1 1 0) and (1 0 0) interfaces have different energies]. This could be caused by the fact that the Cahn–Hilliard model neglects the higher order terms in the Taylor expansion of the free energy with respect to the concentration gradient. In the phase field model of dislocations the order parameter represents the inelastic strain and its gradient becomes a second order derivative of the inelastic displacement. Thus the gradient term in the phase field model is physical rather than phenomenological and improves the accuracy of predicting dislocation core structures as compared with the PN model, as has been shown recently by a comparison between the continuum PN model and its discrete counterpart derived using the lattice Green's function method [245]. It has been shown that the dislocation core width predicted by the Peierls theory is too narrow when compared with experimental measurements [245] and the gradient term has been shown to smooth and widen the core [56,244].

3.3.2.2. Elastic and inelastic energy calculations inside and outside the non-Hookean slab. For a given potential energy surface (PES) such as the GSF energy there are convex and non-convex parts. During deformation strains or displacements that sample the non-convex parts of the PES are called inelastic strains or inelastic displacements, while strains or displacements that sample the convex parts of the PES are called elastic strains or elastic displacements [203]. As mentioned earlier, one of the unique features of the PN model is its partition of a crystal containing dislocations into two parts: Hookean (regions I and III in Fig. 2) and non-Hookean (region II in Fig. 2). In regions I and III the deformation is assumed to be purely elastic and the energy is described by linear elasticity theory. In contrast, there are both elastic and inelastic deformations in region II and the energy is described by the misfit or GSF energy.

In phase field models of dislocations the degrees of freedom in the crystalline and elastic energy are the eigenstrain characterized by the phase field, $\eta(\alpha, m_\alpha, \mathbf{r})$, which is an inelastic strain. In conventional formulations the elastic energy calculation is performed for the entire crystal using linear elasticity theory, including region II, and the crystalline energy is calculated in the entire crystal as well, including regions I and III. Thus the energy in region II in the conventional phase field model contains two contributions: one from the linear elasticity equation and one from the crystalline energy. Similarly, the inelastic strain, with values represented by the phase fields, $\eta(\alpha, m_\alpha, \mathbf{r})$, is allowed to relaxed in the entire crystal rather than being confined to region II. If $\eta(\alpha, m_\alpha, \mathbf{r})$ is not strictly zero outside region II, for example a dislocation core may spread outside the slip plane, then the energy in regions I and III also contains two contributions: one from the linear elasticity equation and one from the crystalline energy.

In a recent effort [246] to make a quantitative comparison between the phase field model and the PN model a new microscopic phase field (MPF) model was developed, in which the crystalline energy was replaced by the GSF energy with its calculation confined to region II and the gradient term was dropped. As can be seen from Fig. 3, as the thickness of the non-Hookean slab decreases in the elastic energy calculation the MPF model prediction asymptotically approaches the prediction of the PN model. Thus, to make the phase field model completely equivalent to the PN model the elastic energy calculation has to be excluded from the non-Hookean slab and the crystalline energy calculation has to be confined to the non-Hookean slab.

3.4. Applications of the MPF model of dislocations

From the above discussion one can see that the MPF model of dislocations is a superset of many previous (semi-)continuum models [1,232,234–236,238–240,247–252] based on the Peierls and Nabarro [1,232,234–236] concepts. As mentioned earlier, the KS microelasticity theory was recently extended to treat inhomogeneous (position-dependent) elastic moduli [58,60–62], which further extends its application to include cracks and voids [70,73,75], free

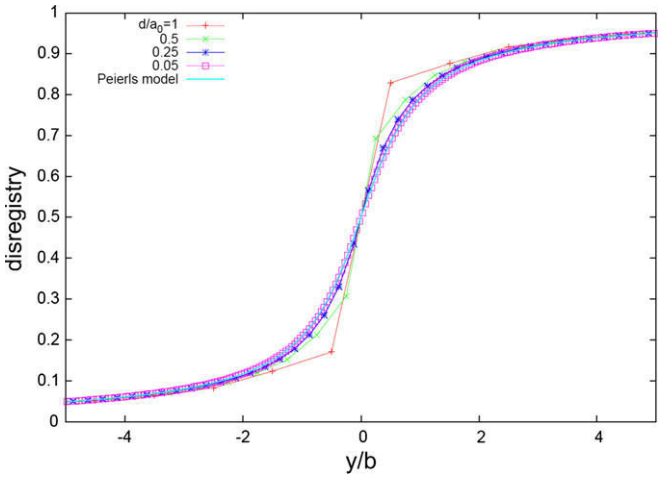

Fig. 3. Quantitative comparison between the microscopic phase field (MPF) model and Peierls–Nabarro (PN) model for predictions of Burgers vector distribution within the core of an edge dislocation in a simple cubic crystal using the same set of input parameters (i.e. sear modulus, Poisson's ratio and misfit energy function). When the thickness d of the non-Hookean slab used in the elastic energy calculation of the MPF model decreased the MPF model prediction asymptotically approached the PN model prediction. a_0 is the lattice parameter.

surfaces [63,68,70,253] and elastically inhomogeneous inclusions [59–62,105,254]. Separation of the material-specific part and the defect configuration-dependent part in the final elastic energy equation (see, for example, Eq. (4)) makes the treatments identical for different types of defects, such as dislocations, impurities, precipitates, surfaces, cracks and voids, and their interactions. Thus, the phase fields contributing to the inelastic strain in general can be any crystalline defects, with their mutual elastic interactions accounted for through the following coupling among their contributions to the inelastic strain field:

$$\varepsilon_{ij}^{T}(\mathbf{r}) = \sum_{p} \varepsilon_{ij}^{T}(\phi_p(\mathbf{r})) \tag{7}$$

which is a linear combination of individual phase fields ϕ, labeled with subscript p, that represents different types of extended defects contributing to the inelastic strain in the system. This treatment provides phase field models with the ability to self-consistently handle the evolution of an arbitrary solid-state microstructure consisting of various stress-carrying defects (see, for example, reviews [154,207]). In the following examples the MPF model is first compared quantitatively with the PN model for prediction of core structures of a straight dislocation in Ni_3Al, using identical GSF energy from *ab initio* calculations as input. Then the ability of the MPF model to treat arbitrary dislocation configurations and dislocation–precipitate interactions is demonstrated.

3.4.1. Dislocation core structure in Ni_3Al

Recently a quantitative comparison between the MPF model and the PN model [246] was carried out for their predictions of the core structure of a $\langle 1\,1\,0\rangle\{1\,1\,1\}$ type straight super-dislocations in Ni_3Al (γ'). Identical model inputs, i.e. the GSF energy and the anisotropic elastic constants from Schoeck, Kohlhammer, and Fähnle [255], were used in the calculations. Fig. 4 shows a comparison between the results obtained using the two models. In the MPF calculations the elastic energy calculation is excluded from the non-Hookean slab (region II in Fig. 2), the inelastic relaxation was confined to the non-Hookean slab and the gradient term was ignored. As can be seen from Fig. 4, complete agreement between the MPF model prediction and the PN model prediction was achieved. The dislocation core in equilibrium exhibited a fourfold extended structure, for both the edge and screw types,

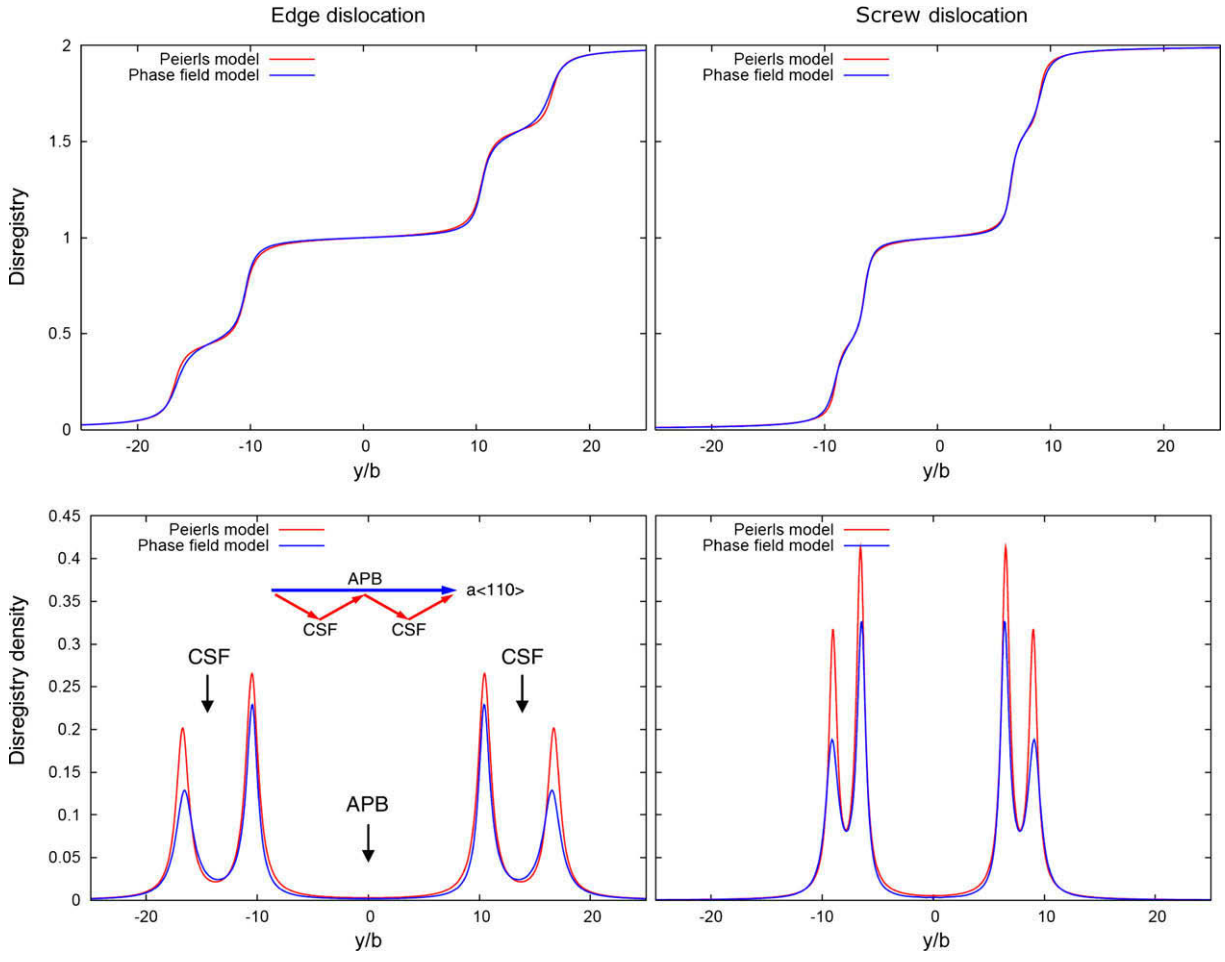

Fig. 4. Core structures of $\langle 1\,1\,0\rangle\{1\,1\,1\}$ edge and screw dislocations in Ni_3Al and comparison with solutions from Peierls model (courtesy of professor Gunther Schoeck). Both calculations used the same input GSF energy and elastic moduli. $b = a_0/2$, with a_0 being the lattice parameter [247].

consisting of two complex stacking faults (CSFs) and one anti-phase boundary (APB), as shown in the inset in Fig. 4.

3.4.2. Structure of a (1 1 1) twist boundary in Al

The above example showed that in the degenerate case of straight dislocations the MPF and PN models predict exactly the same core structures using indentical model inputs. When curved dislocation lines are considered, however, the log(r) type kernel in the PN model is no longer applicable, but the phase field energy function is. To show that the phase field model is a three-dimensional generalization of the PN model, the MPF model was recently applied to study the structure and energy of a complex dislocation assembly–dislocation network formed in a (1 1 1) pure twist boundary in Al [246]. The GSF energy and elastic constants of Al are from Lu et al.[256]. Fig. 5 shows the equilibrium structure of the twist boundary. The shades of gray (color online) represent the misfit or crystalline energy density. The alternative contracted and extended notes and the hexagonal network agree well with the experimental observations [257]. Extension of the model to heterophase interfaces should be straightforward.

3.4.3. Shearing of the γ′-particle in Ni–Al

One advantage of the phase field method in treating dislocation–precipitate interactions is its ability to handle arbitrary configurations of both dislocation and precipitate microstructures, non-singular dislocation cores, dislocation

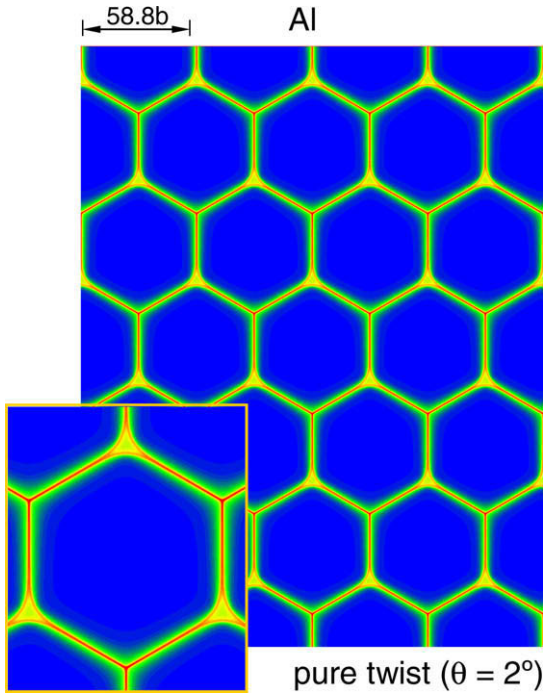

Fig. 5. Structure (misfit energy plot) of a (1 1 1) pure screw twist boundary ($\theta = 2°$) in Al predicted by the microscopic phase field model using the *ab initio* GSF energy as the model input. The inset is an enlarged view of the extended and constricted nodes [247]. (For interpretation to colours in this figure, the reader is referred to the web version of this paper.)

dissociation and stacking fault formation and anisotropic elasticity. Incorporation of *ab initio* γ-surface data into the MPF model has made it possible to quantitatively study dislocation dissociation and formation of various planar faults in complicated γ/γ' two-phase microstructures in Ni-based superalloys. Fig. 6 shows an example of MPF simulations of decorrelated motion of a $1/2\langle 1\,1\,0\rangle$ screw dislocation through a typical bimodal γ/γ' microstructure in a Ni-based superalloy (Fig. 6a) and its comparison with experimental observations at an early stage in a creep test in a recent study on alloy ME3/Rene104 (Fig. 6b) [102,225,258]. The simulation cell contains a periodic array of coarse (secondary) γ'-particles (300 nm) separated by γ-channels (75 nm), randomly dispersed fine (tertiary) γ'-particles (~10 nm) and a $1/2\langle 1\,1\,0\rangle$ screw dislocation, initially placed on the left. A parametric simulation study has documented critical microstructure features, deformation conditions and fault energies that favor the decorrelation, which ultimately leads to microtwinning, versus various faulting modes of deformation. For example, decorrelation of the $1/2\langle 1\,1\,0\rangle$ dislocation into Shockley partials at the entrance of the γ-channel shown in Fig. 6a is driven by the direction of the applied stress, which differentiates the resolved shear stress on the two Shockley partial Burgers vectors, and facilitated by the relatively low intrinsic stacking fault (ISF) energy of the γ phase (10 mJ m^{-2}). The width of the γ-channel in the meantime acts as a threshold that determines whether both partials or only one of them can pass through under a particular applied stress magnitude. The presence of the tertiary particles offers an additional impediment to dislocation motion as CSFs and APBs, respectively, are created in the wake of the leading and trailing Shockley partial dislocations.

3.4.4. Peierls stress for dislocation and boundary migration

In its current formulation the phase field method does not describe lattice friction (the Peierls stress) because all energy terms are expressed in integral forms. For this reason only the equilibrium configurations have been considered so far. However, the Peierls stress has been included in the framework of the PN model by considering lattice discreteness in calculation of the misfit energy [232–236,238,240]. The corresponding modification of the MPF model and calculations of the Peierls stress for dislocations and grain boundaries (such as that shown in Fig. 5) should be straightforward.

It is worth noting that application of the MPF models in the above examples is fundamentally different from the use of the CGPF model of dislocations. The MPF models directly utilize *ab initio* calculations of GSF energies and hence are able to make predictions of dislocation core structure and energy and complicated dislocation configurations without any a priori assumptions. Over the past decade the CGPF model of dislocations has enjoyed an ability to self-consistently handle the complicated geometry of dislocations, their topological changes and their interactions with other extended defects, such as precipitates, grain boundaries and surfaces in three-dimensional elasti-

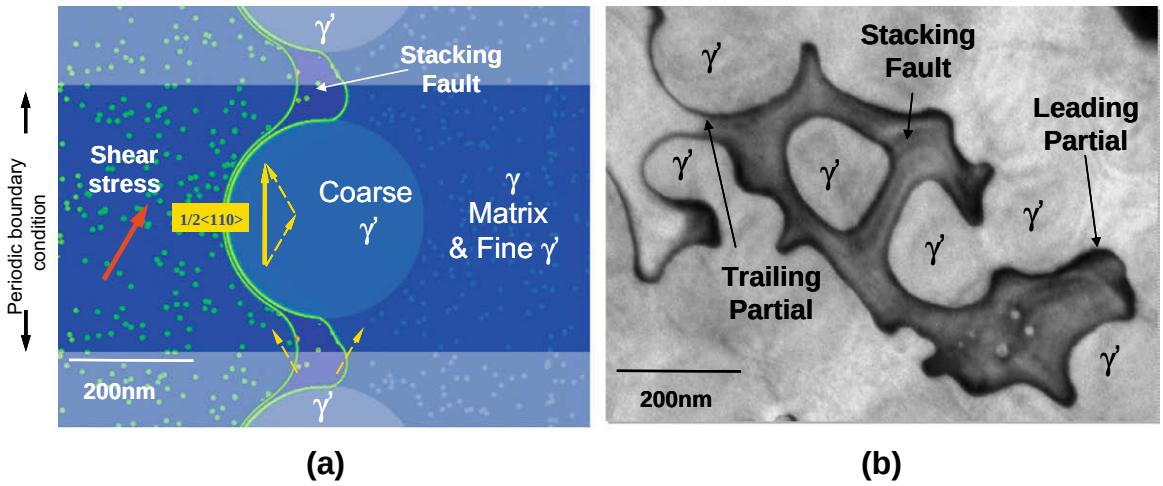

Fig. 6. (a) Phase field simulation and (b) experimental observation (courtesy of R. Unocic and M.J. Mills) of decorrelation of a i/2⟨1 1 0⟩ dislocation into Shockley partial dislocations at the entrance of a γ-channel between two secondary γ' particles [102,259].

cally anisotropic media (for recent reviews, see [70,207]). At such length scales, however, the CGPF model suffers from the same problem as other continuum CGPF models, i.e. loosing the intrinsic ability of a diffuse interface model to predict the fundamental properties of the defects, such as core size and energy, critical nucleus configuration and activation energy of dislocations. Quantitative phase field modeling of dislocation dynamics on the coarse grained level will require similar scrutiny as the other CGPF models discussed earlier in Section 2.3.

4. Microscopic phase field models of deformation twinning and structural transformations

Based on the kinship among dislocation loops, deformation twins and martensitic platelets, attempts are being made [201,202,246] to formulate microscopic phase field (MPF) models of deformation twining and martensitic transformations on an equal footing with the MPF model of dislocations in order to utilize recent *ab initio* calculations of twinning and transformation pathways [176,203–205,259–262].

4.1. MGSF energy landscape for deformation twinning

The MGSF energy landscapes along the deformation twinning energy path in fcc and bcc metals have been probed by *ab initio* calculations [203], which causes twinning shear of the unit cell in a primarily layer-by-layer fashion. Tadmor et al. introduced a new material concept called twinnability [252], which is the ratio of γ_{us}, the unstable stacking fault energy (0 → 1 barrier in Fig. 7a and b), to γ_{ut}, the unstable twinning energy (1 → 2 barrier in Fig. 7a and b), and have evaluated it for fcc metals [263]. DFT calculation of the (1 1 2)⟨1 1 1⟩ twinning MGSF energy of bcc Mo [203] showed dramatically different features (Fig. 7c and d). The thinnest metastable twin was two layers. Three and four layer twin embryos were unstable. This means that if one looks at nucleation of deformation twins in bcc Mo the first critical event must be simultaneous emission of two partials together (group A). The next critical event must be simultaneous emission of an additional three partials (group B), on top of A. Only then can the twin assume layer-by-layer growth. This is clearly a very different process from fcc deformation twinning [264–266] and must lead to different minimum energy paths (MEP) [203]. At present no interatomic potential can give long-range MGSF behavior such as Fig. 7d, so using MPF with *ab initio* inputs provides a viable option if one wants to calculate the MEPs [203] of heterogeneous twin nucleation [252,264] in bcc metals.

Not only nucleation, but also the growth processes of deformation twins in bcc Mo are intriguing. DFT results [203] indicated that the twin boundary migration energy of Mo is extremely small (40 mJ m^{-2}), which is only one-third of that of Al, while Mo has five times the affine shear modulus of Al. According to the PN model, twin partial dislocations in Mo must have very wide cores and high mobility. The stress to homogeneously nucleate [119] a twin partial loop on the face of a thick enough twin is only 1.4 GPa, which is really small with reference to the bulk flow critical resolved shear stress of Mo of 750 MPa [267]. This calls into question the necessity of classic deformation twin growth mechanisms like the Cottrell–Bilby and double cross-slip [268,269] mechanisms for bcc Mo, since only a small stress concentrator or perhaps thermal fluctuation is needed to induce homogeneous nucleation [14] of a partial loop on a "thick enough" twin, which was estimated to be five layers. Clearly, this treasure trove of *ab initio* information could be incorporated in properly formulated MPF calculations. The nucleation and mobility of conventional dislocations have been subjected to intense scrutiny at both the atomistic and field theoretic levels [14,225]. The same cannot be said for deformation twinning and martensitic transformations, although a close kinship among twinning, martensitic transformations and conventional dislocation plasticity is well acknowledged.

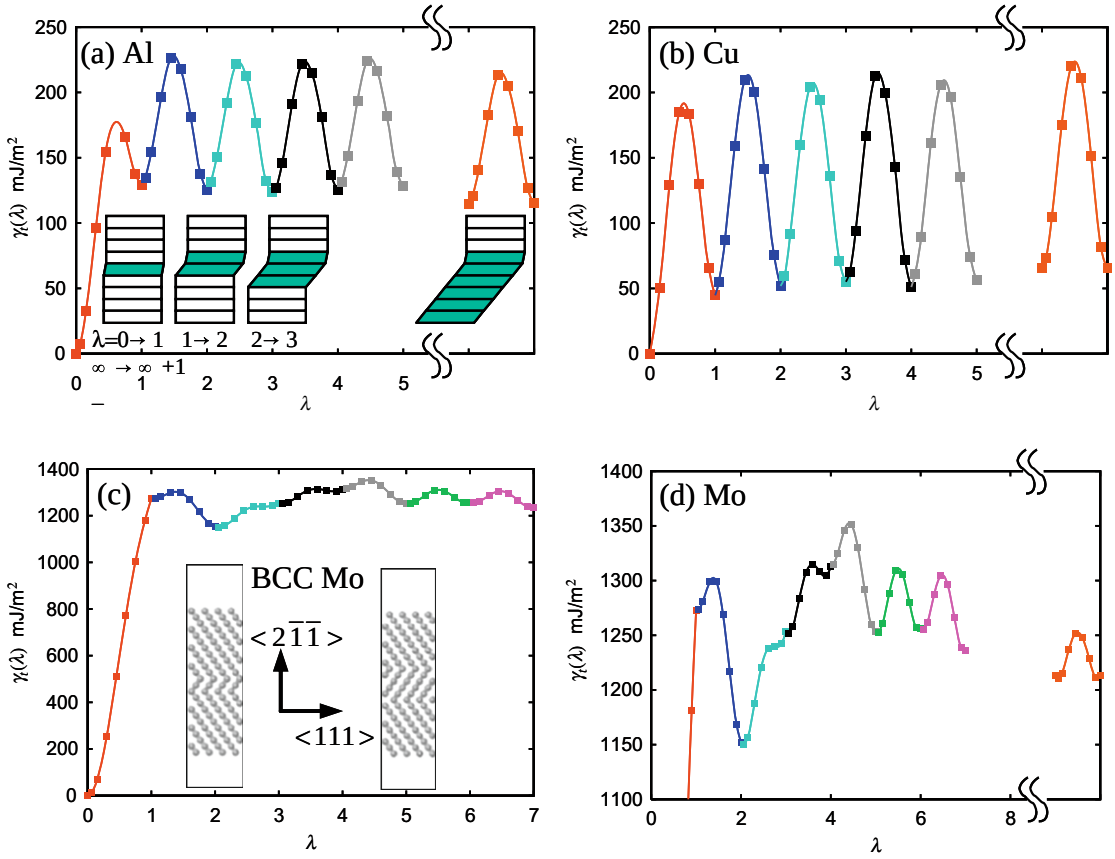

Fig. 7. (a) $(1\,1\,1)\langle 1\,1\,2\rangle$ twinning MGSF in fcc Al, calculated using DFT [176,203]. $\lambda = n$ corresponds to an n-layer twin embryo, while $\lambda = (n, n+1)$ corresponds to shearing the $n+1$th atomic plane by $(\lambda - n)\mathbf{b}_p$. The profile on the far right corresponds to the $n \to \infty$ limit (twin boundary migration). (b) The same pathway in fcc Cu. Note that both Al and Cu have stable twin embryos at all integers n. (c) $(1\,1\,2)\langle 1\,1\,1\rangle$ twinning MGSF in bcc Mo. (d) Magnified view. Note that $n = 2, 5, 6, \ldots$ are metastable minima, while $n = 1, 3, 4$ are unstable [203]. A steady-state oscillatory pattern does not set in until $n = 5$.

4.2. MEP-MGSF landscape for martensitic transformations

In the theory of martensitic transformations the chemical free energy, which is the counterpart of the crystalline energy in the theory of dislocations, is usually approximated by Landau free energy polynomials [270,271], which are power series expansions with respect to a chosen set of order parameters. The form of the polynomials is dictated by free energy invariance under symmetry operations and the nature of the transformations (such as first order versus higher orders and proper versus improper, etc.). The Landau polynomial typically takes the form 2-3-4 for proper martensitic transformations and the form 2-4-6 for improper martensitic transformations. The primary order parameter is an affine strain (homogeneous lattice strain) in the former and a long-range order parameter characterizing atomic displacement within a unit cell (i.e. shuffle) in the latter. A typical example of the order parameters for a proper martensitic transformation is the pure tetragonal strain (Bain strain) associated with the fcc → bcc transformation [272,273]. Its values represent homogeneous lattice distortions of finite volume elements of the fcc phase to the bcc phase along the Bain path. A typical example of the order parameters for an improper martensitic transformation is the amplitudes of "soft" optical modes that result in the mutual displacement of atoms within a unit cell of the parent phase, as in partially stabilized zirconium.

The Landau theory of phase transitions and Landau expansion polynomials [270,271] have been widely used in phase field simulations of martensitic transformations (for a recent review, see [201] and references therein) and other structural transformations. A great advantage of the Landau theory is its amenability to qualitative parametric studies, because it uses as input only low-dimensional energy functions (i.e. the Landau expansion polynomials) of a predetermined set of order parameters, instead of the full potential energy surface in the entire configuration space. To make the theory quantitative, however, one needs first to validate that the transformation path defined by the predetermined order parameters (such as the "proportional strain" and "sequential shear" paths and load–path bifurcations discussed in [274]) actually corresponds to the MEP, then to formulate a Landau polynomial with appropriate order parameters and, finally, to parameterize the expansion coefficients, all by *ab initio* calculations. The Bain path in fcc → bcc martensitic

transformations has been shown by atomistic calculations using empirical potentials [275] to correspond closely to the MEP that connects the two local minima (corresponding to the fcc and bcc structures) on the potential energy surface and many *ab initio* calculations were limited to the Bain path (see, for example, [261] and references therein). However, recent *ab initio* calculations [204,205,259] have shown general non-linear paths in the strain space. Since the accuracy of the potential energy hump along the MEP between the parent and product phases determines the accuracy of the interfacial energy and the path itself determines the elastic strain relaxation, both of which are critical in determining the activation energy for nucleation [276], it is critical for any model not to have any a priori constraint about the transformation path.

As shown in the preceeding section, the extension of GSF energy to MGSF energy has allowed studies of deformation twinning via *ab initio* calculations. Since deformation twinning can be regarded as a special case of martensitic transformation [264], further extension of the MGSF energy to include shuffle and possible dilatational strains would allow one to quantitatively describe martensitic transformations and other shear-dominated processes using MPF models with *ab initio* calculations as inputs.

Different from dislocations and deformation twinning, additional internal displacements (shuffling) will accompany the affine deformation of each unit cell in martensitic transformations. The shuffling degrees of freedom and the affine strain degrees of freedom, plus possible coupling between different layers [176,203] (sometimes called "synchroshear" [277–279]), constitute a high-dimensional energy landscape for which an explicit representation is often not possible. For instance, the general strain space is six-dimensional; suppose that there are three extra shuffling degrees of freedom, then the microscopic energy landscape of such a general martensitic transformation will be at least nine-dimensional (if different transforming layers are decoupled [176,203]). Clearly, this brute force approach would be untenable for general problems. The so-called reaction coordinate (ξ) representation of MGSF will reduce the nine-dimensional energy landscape to a one-dimensional function, by sampling the lowest saddle energy path (minimum energy path, MEP) in the nine-dimensional space [204,205,259] that connects the initial metastable state (parent lattice) with the final metastable state (product lattice). In essence, the MEP on the MGSF energy surface (MEP-MGSF) is an optimal one-dimensional sampling of the nine-dimensional energy landscape, which the martensitic transformation is likely to follow microscopically at the unit cell level. This path will in general not be straight in the nine-dimensional space and in fact can be quite curved or even kinked [204,205,259]. The proper utilization of such a MEP-MGSF in the context of MPF simulations is called the reaction coordinate theory of martensitic transformations [246]. The *ab initio* calculation of MEP-MGSF has been implemented in the planewave density functional theory program VASP [176,203,243], where the MEP of the MGSF is searched using the NEB technique in the general space where unit cell shape and internal coordinates are treated on an equal footing mathematically and can vary simultaneously with no constraints, unlike the other existing approaches [204,205,259]. In a chemically non-uniform system, caused by the presence of either antisite atoms or impurities, the MEP-MGSF energy will be a function of the local defect concentration [235,259].

4.3. Critical nucleus configuration and activation energy

Since microstructural features developed during solid-state reactions (e.g. phase transformations, plastic deformation, fracture, etc.) are often influenced by long-range elastic strain fields that are in general functions of size, shape, spatial orientation and mutual arrangement of all stress-carrying defects (dislocations, precipitates, cracks, etc.) [228], a rigorous treatment of nucleation in solids requires a self-consistent description of interactions between a nucleus and pre-existing microstructural constituents without any a priori assumptions. Since the phase field method has been shown to be a superset of the Cahn–Hilliard description of chemical inhomogeneities [164] and the Peierls (cohesive zone) description of displacive inhomogeneities [247], the phase field total free energy function is able to describe nucleation of various types of extended defects produced by both diffusional and displacive [170,228,248,274,280–292] processes that produce, respectively, chemical and structural non-uniformities. It has been demonstrated [170,283] that within the limits of little supersaturation or a low driving force the non-classical theory reproduces all the features predicted by classical nucleation theory. However, the difficulty of this approach is locating the exact saddle point in a configuration space of very high dimensions. Analytical or semi-analytical solutions are available only in a much reduced configuration space (e.g. one-dimensional problems) [170,228,274,283] or in the asymptotic limit of vanishing metastability of the parent phase [289], and numerical solutions [293,294] are generally expensive and less stable because the saddle point is an unstable stationary point. For the same reason, the Langevin dynamic equations [146–148,237,293,295–297] are incapable of obtaining the exact solutions [202].

Taking advantages of the generality of the phase field total free energy function (in particular its ability to describe arbitrary non-uniformities in the presence of long-range interactions and anisotropies), several new approaches [202,298,299] were recently developed to accurately determine the critical nucleus configuration of a thermally activated process by combining phase field energetics with saddle point search algorithms. Of particular interest [202] is the combination of the free end nudged elastic band (FE-NEB) method [300] that allows an efficient saddle point search along MEPs and the Langevin force approach that provides the free end configuration for the FE-NEB method. The NEB [301] calculations require only the total

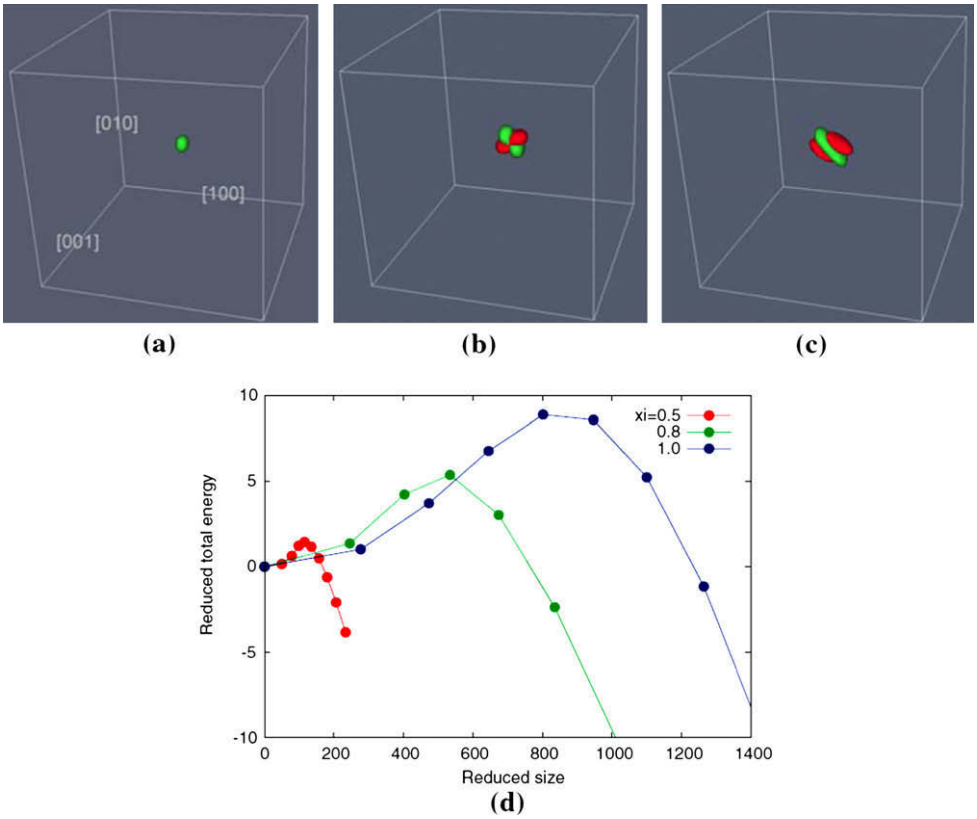

Fig. 8. Transition of the critical nucleus from a single variant to a two-variant configuration with increasing elastic energy contribution or decreasing chemical driving force: (a) $\xi = \mu\varepsilon_0^2/\Delta f_0 = 0.5$, (b) $\xi = 0.8$ and (c) $\xi = 1.0$, where μ is the shear modulus, ε_0 is the typical value of misfit strain and Δf_0 is the chemical driving force for the transformation. The corresponding nucleation barriers are shown in (d) [202].

free energy and its first order derivatives (variations), which are straightforward and inexpensive to obtain from a phase field model. This approach has been previously implemented for dislocation level plasticity studies [225]. Application [202] of the new approach to a generic cubic → tetragonal structural transformation showed immediately non-trivial results (Fig. 8): an interesting critical nucleus configuration akin to neither the parent phase nor the fully grown product phase was observed (Fig. 8b). The result was produced using a compromise between the interfacial energy and the elastic strain energy of the critical nucleus. The method is applicable to thermally activated processes involving both chemical and structural non-uniformities, such as nucleation of stacking faults and dislocation loops [225], voids and microcracks and ferroelectric and ferromagnetic domains. It is able to treat heterogeneous nucleation near arbitrary pre-existing defects.

5. Phase field models of fracture

The concept of a crack defect in linear elastic fracture mechanics [302] is similar to a Volterra dislocation, i.e. it is an infinitely narrow line singularity. From a continuum mechanics perspective, mode II/III cracks differ from edge/screw dislocations only in the sense that after the line singularity has swept past a material area, in the case of dislocation there is 100% recovery of traction across the area, since the reconstructed material is still a perfect crystal after a shift by a perfect Burgers vector, whereas in the case of a crack there is 0% recovery of the traction force, as a traction-free boundary condition is imposed on the newly created surfaces. Thus, the difference between a dislocation and a crack is essentially only in the non-linear portion of the traction–displacement relation. In the former case, a r^{-1} type stress singularity develops as one approaches the line defect. In the latter case, a $r^{-1/2}$ type stress singularity develops, whose amplitude is proportional to the external driving force (a crack is usually much "larger" than a dislocation because its existence is predicated upon external loading, otherwise the crack would heal). Stress in real materials can be very high, but not infinite [303]. The regularization of the crack tip stress field proceeds in a similar fashion to Peierls' treatment of the dislocation core: a certain kind of non-linear, non-convex response must be imposed in the high stress regions, coupled with a majority of elastically stressed material. In order to achieve traction-free boundary conditions physically, some kind of mode I separation displacement may exist in the material at the microscopic level, even for mostly mode II and III cracks. The so-called cohesive zone model was developed conceptually [178–180] and numerically [181–186] to accomplish this effective "cohesive separation" response. Note that plasticity may play an important role in the cohesive zone, illustrated by the Hutchinson–Rice–Rosengren crack tip solution

[304,305] for power law hardening materials. Even a nominally brittle material may manifest flow and ductility on the nanoscale [306,307]. Thus, the lengthscale of the effective cohesive separation may be significantly larger than the interatomic spacing [308]: imagine nanoscale ligaments pulling on the crack surfaces trying to close the crack.

Similar to Nabarro's treatment of lattice trapping of dislocations by discrete atom sampling [232], there is also lattice trapping of brittle crack movement [309,310]. Also, coupling between crack tip stress and plasticity is a subject of considerable interest in the study of fractures. Nucleation of a single dislocation from a crack tip was first studied by Rice et al. using a Peierls like model [247–249], followed by numerical simulations by Xu et al. [250,251]. All these treatments have strong similarities with the MPF approach to dislocations described previously. One technical challenge was the incorporation of traction-free boundary conditions, since it implies the embedding of a zero modulus region, in contrast to a 100% traction recovery response for dislocations, where one can use the inhomogeneous transformation strain with a homogeneous modulus approach [50,54]. However, this difficulty has been removed by using an iterative algorithm to model elastic inhomogeneity [60–62,242] exactly in the phase field method. The interactions of dislocations and martensites with free surfaces, voids and cracks have been demonstrated to work robustly in the phase field [63,68,70,73–75,253]. Thus, fundamentally there is no great obstacle to modeling cracks and fractures on an equal footing to dislocations, martensites and plasticity. The treatment of bulk diffusion and surface diffusion with moving boundaries are less of a computational challenge in phase field modeling, because it is not a boundary tracking method [77,85–87,311,312].

Crack nucleation in two-dimensions has been modeled using a continuum field approach similar to the Peierls model with a saddle point search [284]. Crack path selection, crack branching and the energy dissipation rate in crack propagation have been investigated in detail by the phase field method, taking into account elastic and surface energy anisotropies [79,81–83,88,89]. Dynamic crack propagation [313] has been modeled, incorporating elastodynamic inertia effects [84]. Chemical interactions such as hydrogen diffusion and hydrogen-induced decohesion have been modeled, where the crack tip stress field plays a critical role in biasing diffusion [85,86]. The coupling of crack tip stress to other order parameters, such as ferroelectric domain switching and transformation toughening, have also been modeled [314,315]. Fracture is generally a very complex phenomenon. The versatility of the phase field approach in treating the plethora of microstructural and chemical interactions [70,74,77–89] make it a powerful tool for future modeling of fractures.

6. Modeling coupled displacive–diffusional deformations

Phase transformations are generally classified into diffusional and displacive transformations and hybridization of the two [316], such as the austenite → bainite transformation. Deformation mechanisms are similarly classified [317]. Well-known examples of diffusion-aided deformation include Nabarro–Herring [318] and Coble [319] creep, power law creep involving dislocation climb [320], sintering [321], Asaro–Tiller–Grinfeld instability [77,87,311,322–324], electromigration [71–73,75,76], etc. Other processes, such as solute drag on dislocation motion [325] and dynamic strain aging [326] and hydrogen embrittlement [327,328], also involve coupled chemical and displacive characteristics. All these processes are amenable to both MPF and CGPF simulations. The following examples demonstrate such phase field simulations for dislocation-induced γ' rafting and creep deformation in Ni-based superalloys.

Dislocation filling in γ-channels and γ' rafting (directional coarsening) are the major microscopic processes taking place during high temperature creep deformation of single crystal Ni-based superalloys [99,100], which control the lifetime of the blades in jet engines. These two processes are dynamically linked, providing a typical example of displacive–diffusionally coupled processes. Under a given external load dislocations preferably enter certain γ-channels and alter the coherency state and energy of γ/γ' interfaces and local stress fields, creating chemical potential gradients among different γ-channels that drive diffusive flow and morphological changes in the γ/γ' microstructure. In turn, changes in particle shape and the coherency state of the interface alter the local stress state and thereby the Peach–Koehler force exerted on dislocations. Many previous models have treated these two processes separately, without capturing the dynamic coupling. The phase field models [103–107] offer an opportunity to treat them simultaneously in a common framework. The recent works by Zhou et. al. [103,105–107] considered a pseudo-binary Ni–Al single crystal at two different length scales, with one tracking inelastic strain fields of individual dislocations on discrete slip planes and the other tracking continuously distributed plastic strain fields created by dislocations from different active slip systems.

6.1. Dislocation–γ' interaction and γ' rafting

Since the lengthscale relevant to coarsening is associated with the typical diffusion field and the size of precipitates (~400 nm), the microscopic details such as dislocation core structure need to be 'coarse grained' out by using the gradient term of the phase fields as in the conventional phase field models. The choice of the gradient term coefficient is determined by making the dislocation core numerically smooth on the mesoscale computational grid. In the example considered in Zhou et al. [103] the effective core width is about 20 nm, with a grid size of 6.6 nm. In the simulations equilibrium dislocation configurations corresponding to the initial γ/γ' microstructure under a given applied load and lattice misfit between the γ and γ' phases were first established, by evolving only the order parameters for

dislocations following the time-dependent Ginsburg–Landau equation [147,189]. Then the dislocation cores were restored to sharp cores and the stress fields associated with the dislocations were calculated. The γ/γ' microstructure was then evolved using the Cahn–Hilliard equation [188] under the stress fields from both lattice misfit between the γ and γ' phases and channel dislocations. Upon the change in the γ/γ' microstructure the channel dislocation configurations were evolved instantaneously.

The elastic interaction between the γ/γ' microstructure and the channel dislocations was considered through coupling between the inelastic strains associated with the two types of defects:

$$\varepsilon^0_{ij}(\mathbf{r}) = \frac{2(a_{\gamma'} - a_\gamma)}{(a_{\gamma'} + a_\gamma)(c^{eq}_{\gamma'} - c^{eq}_{\gamma})}\left[c(\mathbf{r}) - c^{eq}_{\gamma}\right]\delta_{ij} + \sum_q \frac{\mathbf{b}_0(q)\otimes\mathbf{n}(q) + \mathbf{n}(q)\otimes\mathbf{b}_0(q)}{2d(q)}\eta_q(\mathbf{r}) \quad (8)$$

The first term on the right-hand side of Eq. (8) is from the lattice misfit between $\gamma(a_\gamma)$ and $\gamma'(a_{\gamma'})$ phases. δ_{ij} is the Kronecker delta and represents a dilatational strain tensor. c^{eq}_{γ} and $c^{eq}_{\gamma'}$ are, respectively, the equilibrium compositions of the γ and γ' phases. The second term represents the inelastic strains from individual dislocations (characterized by η_q) from slip systems defined by the Burgers vector $\mathbf{b}_0(q)$ (in a form of $a/2\langle 1\,1\,0\rangle$, with a being the lattice parameter) and slip plane normal $\mathbf{n}(q)$. It should be noted that the two inelastic strain terms in Eq. (8) account for not only the elastic interaction between the respective defects (i.e. precipitate–precipitate and dislocation–dislocation), but also their mutual interactions through the total elastic energy.

Under 152 MPa [107] uniaxial load among the 12 primary $1/2\langle 1\,1\,0\rangle\{1\,1\,1\}$slip systems only eight have non-zero resolved stress components. Additionally, the coherency stress of the γ/γ' microstructure further differentiates the activities of the eight slip systems into three types of $\langle 1\,1\,0\rangle$ oriented γ-channels (see, for example, Fig. 9). As a consequence, the chemical potentials in different γ-channels are different, driving diffusional fluxes that cause some of the γ-channels to close up and others to open up. Eventually, plate-type (N-type) and rod-type (P-type) rafted γ' microstructures were developed (Fig. 9).

6.2. γ' rafting and creep deformation

To account for statistical variations in size, shape and spatial distribution of γ' precipitates the model of dislocation–microstructure interaction in the above example was extended to a larger lengthscale close to experimental observations of rafted γ' microstructures. Major modifications were made to both the dislocation and the γ/γ' microstructure models [107]. First, the phase fields, which were originally defined to characterize inelastic strain fields of individual dislocations on discrete slip planes, were replaced by new phase fields that describe plastic strain fields distributed continuously in space (Fig. 10). The crystalline energy that originally carried the periodic interatomic potential with respect to inelastic displacement (or

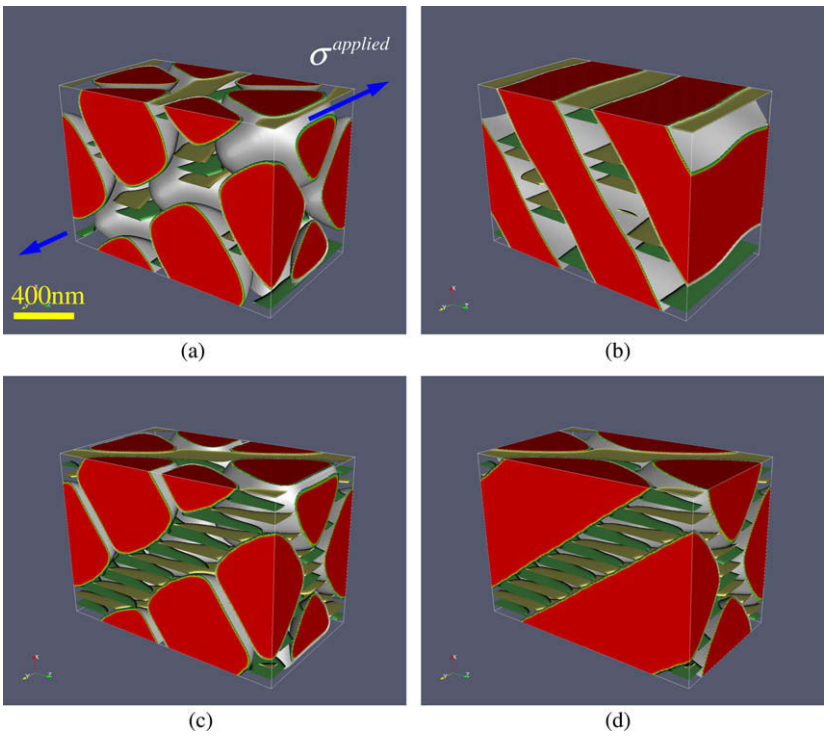

Fig. 9. Formation of an N-type raft at: (a) 3.6 h and (b) 10.7 h in an alloy with −0.3% lattice misfit and a P-type raft at (c) 3.6 h and (d) 7.2 h with +0.3% lattice misfit, under 152 MPa tensile stress along the [0 0 1] direction [103].

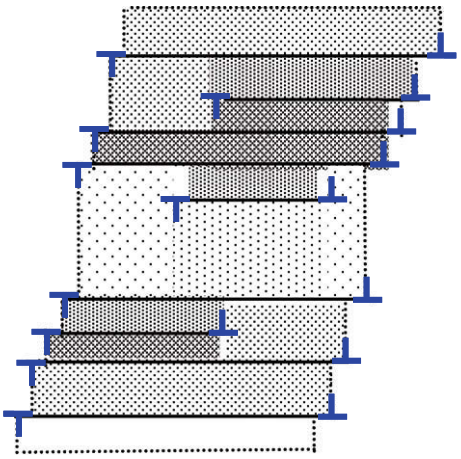

Fig. 10. Discrete dislocations and a continuum field of inelastic (plastic) strain field (dotted and shadowed regions) that yields the same plastic deformation on the coarse grained lengthscale (much greater than the dislocation core size).

disregistry) was, by coarse graining, converted to a constant averaged potential energy that only renormalizes the total energy. Second, the γ/γ' microstructure evolution incorporated the model of Kim et al. [216] to allow for the treatment of solute diffusion at an increased lengthscale without artificially altering the driving forces for precipitate growth and coarsening. Accordingly, the chemical free energy for γ/γ' phases was chosen in the form of four phenomenological order parameters to characterize the γ and γ' phases and the four types of anti-phase domain in γ'. While the individual free energies of the γ and γ' phase could have been imported from the CALPHAD database for specific alloys, only fitted parabolic polynomials were used in this study as the simulated microstructure is in a coarsening stage, where solute concentration variations in γ and γ' are around the equilibrium compositions of the two phases.

Fig. 11 shows the simulated rafting microstructures with positive and negative lattice misfits. The simulation cell linear dimension is 5 μm, with a grid size of 20 nm. The initial microstructure (Fig. 11a) was generated by phase field simulation of the aging process of an alloy having a −0.3% lattice misfit at 1300 K for 4.7 h without external load. Besides the development of similar N-type and P-type rafting morphologies under uniaxial load conditions, as in the previous example, the microstructures (Fig. 11b and c)

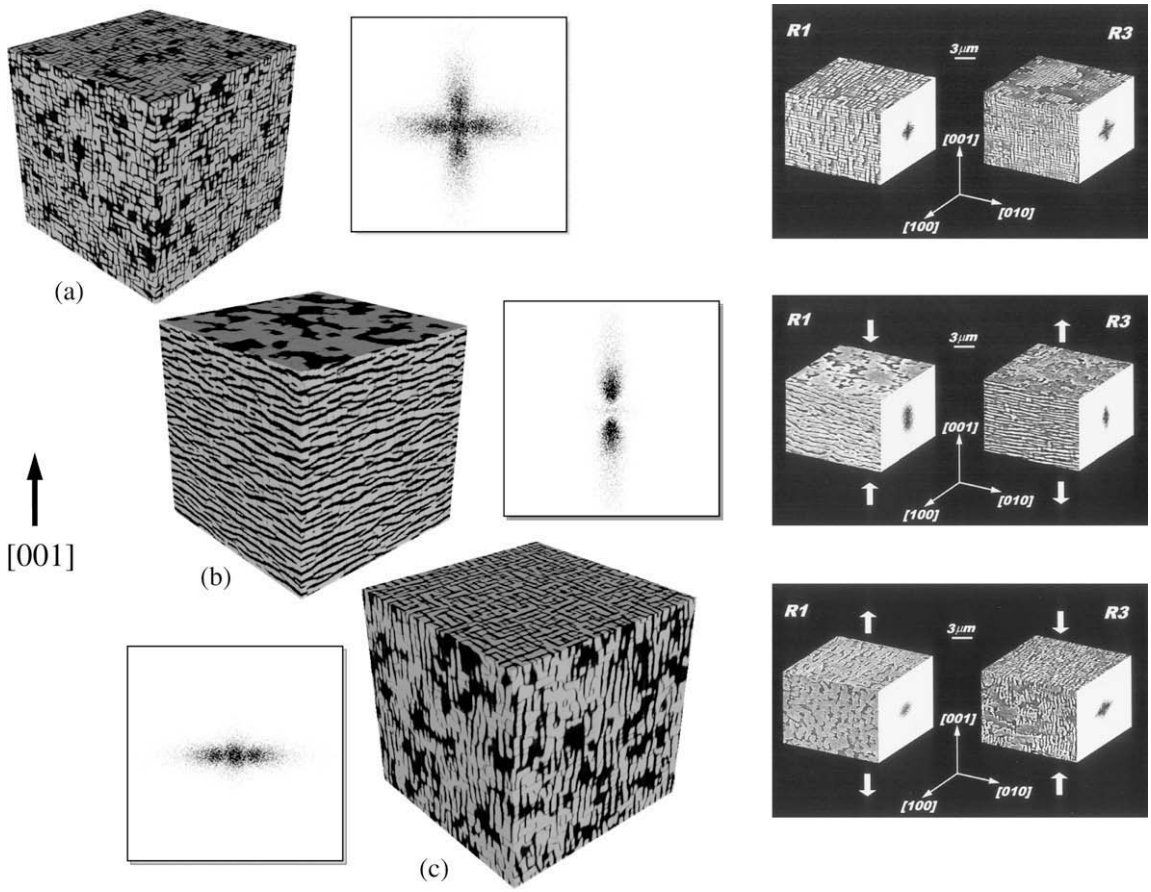

Fig. 11. (a) Simulated γ/γ' microstructures with ±0.3% lattice misfit and no external load, aged at 1300 K for 4.7 h. Rafted microstructures developed from: (a) after an additional 5.6 h ageing under 152 MPa tensile stress along [0 0 1] by assuming the lattice misfit of (b) to be −0.3% and (c) +0.3% [102]. The inset shows the Fourier transform (diffraction pattern) of the corresponding microstructure. The images on the right are from experimental observations under similar conditions [331].

simulated at such lengthscale show a remarkable resemblance to those (images on the right in Fig. 11) observed in experiments [329] regarding both microstructure morphologies and timescale. The rafting kinetics, precipitate–matrix inversion process and the corresponding creep deformation have been characterized with respect to parameters such as applied stress and lattice misfit.

Even though phase field simulations at such length scales are amenable to parametric studies exploring the effect of alloy chemistry and processing and service conditions on γ' rafting kinetics and the corresponding creep deformation, mechanistic studies of many other coupled displacive–diffusional processes require modeling capabilities at atomistic length scales but diffusional timescales. A typical example is the shearing of γ' particles by coupled displacive–diffusional (reordering) processes, including microtwinning, superlattice extrinsic stacking fault shearing and stacking fault ribbon formation, recently discovered in Ni-based superalloys [101,102]. Many other examples exist of displacive–diffusional dual mode structural transformations (such as interface migration by ledge mechanisms) [316]. In this regard, the recently developed phase field crystal (PFC) method offers a unique opportunity.

7. Phase field crystal method

The PFC method was developed by Elder et al. [330,331] to model solid transformations at diffusive timescales, but at a spatial resolution comparable to atomistic simulations [5], incorporating elastic and plastic deformation effects. A similar formulation based on the atomic density field theory generalized from the concentration wave approach to atomic ordering [332–334] was proposed by Jin and Khachaturyan [335]. The PFC method utilizes one particle density

$$\rho(\mathbf{x},t) \equiv \left\langle \sum_{i=1}^{N} \delta(\mathbf{x}-\mathbf{x}_i(t)) \right\rangle \tag{9}$$

as the order parameter field, where N is the number of particles and $\{\mathbf{x}_i(t)\}$ are discrete particle positions at time t. Prior to PFC there was a long history of using single particle density and higher order density correlation functions in the study of simple fluids [336,337]. It can be shown that, parallel to the DFT for electrons [15,338], that the free energy of a classical discrete particles system at thermal equilibrium is a function of its single particle density [339–346]. Van der Waals first formulated a theory of liquid–gas surface tension based on ρ value and density gradient $\nabla\rho$ [162,337,344,347]. For solids, Kirkwood and Monroe initiated the study of solid–liquid interfaces based on a continuous density field [348,349]. Ramakrishnan and Yussouff solved this at freezing temperatures by formulating the problem as a grand canonical ensemble and assuming the direct correlation functions in the crystal and liquid phases to be equal at equal temperature and chemical potential [350] (instead of at equal average density, as assumed by Kirkwood and Monroe [348,349]). Following Ramakrishnan and Yussouff's breakthrough, important work was done along the line of DFT for solids by Haymet and Oxtoby [351–354] and Curtin and Ashcroft [355,356].

The connection between PFC and atomistic simulations was illustrated by Tupper and Grant [357]. Clearly, some kind of ensemble or time averaging is necessary on the right-hand side of Eq. (9), denoted by $\langle\cdot\rangle$, so it can limit towards a spatially smooth field by overlaying snapshots of δ functions, similarly to Born's "probability wave" interpretation of quantum mechanical wave functions.

With time averaging of atomistic trajectories the outcome of Eq. (9) clearly depends on the time averaging (coarse graining) window Δt. In simple monatomic metallic liquids at the melting temperature the self-diffusivity $D_s \approx 10^{-8}\,\mathrm{m^2\,s^{-1}}$: assuming a nearest neighbor distance of $r_0 = 2$ Å, it will take about $t_D = r_0^2/D_s \approx 4$ ps for an atom to diffuse past its original nearest neighbor position. On the other hand, the bond stretch "vibrational period" is estimated to be $t_V \approx 2\pi(mr_0^2/E_B)^{1/2}$, where m is particle mass ≈ 100 amu and E_B is the binding energy due to the interatomic potential $\sim$1 eV, in which case $t_V \approx 1$ ps. Thus diffusive and vibrational motions of an atom in simple liquids cannot be easily separated, and it does not make sense to choose Δt as between t_D and t_V. So one is likely to choose $\Delta t \gg t_D \approx t_V$ in order to obtain a smooth field, in which case the individuality of atoms in a one particle density field is lost due to diffusive mixing. With $\Delta t \gg t_D \approx t_V$ the resulting $\rho(\mathbf{x}, t)$ must be highly uniform if inspected at an atomic wavelength of $\sim r_0$. So, in a quiescent simple fluid, if far from its interfaces, where $\rho(\mathbf{x}, t)$ can change abruptly [16,358], $\rho(\mathbf{x}, t)$ will be a uniform ρ_0. This is the case for a simple monatomic fluid or a "structureless fluid" [359].

The situation with time averaging is quite different for solids, which can be crystalline or amorphous. In simple monatomic metallic crystals at their corresponding melting temperature the self-diffusivity $D_s \approx 10^{-12}\,\mathrm{m^2\,s^{-1}}$, so $t_D = r_0^2/D_s \approx 40$ ns, while t_V is still $\sim$1 ps. Furthermore, D_s drops rapidly with decreasing temperature. So $t_D \gg t_V$, and there is a clear separation of timescales between vibrational and diffusive motion of an atom in the crystalline bulk. The same also holds true for most amorphous solids. One thus has a choice of picking either

$$t_D \gg \Delta t \gg t_V, \tag{10a}$$

or

$$\Delta t \gg t_D \gg t_V. \tag{10b}$$

for time averaging in Eq. (9).

In crystals, for both Eqs. (10a) and (10b), if diffusion occurs by mechanisms that preserve the long-range order of the vibrational site lattice (termed a "network" in [360,361]), such as by vacancy exchange, then $\rho(\mathbf{x}, t)$ resulting from Eq. (9) will preserve strong modulations at atomic wavelengths. Indeed, the Bragg peaks and Debye–Waller factor [362,363] from diffraction experiments directly correspond to such $\rho(\mathbf{x}, t)$ modulation spacing and width, respectively. There may still be coarse grained t-depen-

dence in $\rho(\mathbf{x}, t)$, arising from transformations in solids occurring on much slower timescales than Δt, which would correspond to diffraction pattern changes in *in-situ* diffraction experiments [364,365], but the basic "wavy features" of $\rho(\mathbf{x}, t)$, i.e. long-range order, is robustly preserved with either Eq. (10a) or (10b) coarse graining. One can thus hope to formulate a free energy function based on such robust features of $\rho(\mathbf{x}, t)$ with no ambiguity.

For amorphous solids the time averaging in Eq. (9) is a more sensitive issue, because diffusion can occur by mechanisms that locally destroy the site "network" [360,361]. That is to say, mass transport may not only occur by exchange of matter between "sites", but the vibrational sites themselves could be removed or added. In such case Eqs. (10a) and (10b) time averaging does make a difference. In Eq. (10a) the "wavy features" of $\rho(\mathbf{x}, t)$ is preserved, as one coarse grains over vibrational motion only, whereas in Eq. (10b) one runs the risk of losing the wavy features, as in liquids. Thus, in order to formulate a free energy function for amorphous materials, which does not have long-range order, one must state from which time averaging scheme, Eqs. (10a), (10b), the dependent field $\rho(\mathbf{x}, t)$ is derived, since the two schemes lead to fundamentally different $\rho(\mathbf{x}, t)$. The difference in the free energies can be shown to be proportional to the residual entropy of the glass. This subtlety can be important even for crystalline solids, since the in-plane atomic structures of many crystal grain boundaries and crystal–crystal phase boundaries may be regarded as "random" or "amorphous", with no long-range order. The spatial and temporal domains of validity of PFC simulation have been explored based on the Poisson bracket formalism by Majaniemi et al. [366,367].

For systems at complete equilibrium, assuming ergodicity, time averaging is the same as ensemble averaging, and one will only obtain a time-independent field $\rho(\mathbf{x})$ from Eq. (9), and formulate a free energy function with it. However, most often we are interested in materials kinetics problems where a local equilibrium is reached at some small length-scale but the system is out of equilibrium at some coarser length scales. To monitor the evolution of $\rho(\mathbf{x}, t)$ one thus needs to formulate an equivalent time-dependent density function theory (TDDFT) [368] for classical discrete particles system. There is no reason to suspect that for weakly out of equilibrium systems Onsager's linear response and the Cahn–Hilliard formalism for conserved fields [361] would not work for the density field. So the evolution equation formulated by Elder et al. [330,331] is conventional, as is the typical phase field approach. The novelty of the PFC method lies in its adaptation of the atomic density wave [335,369] as the order parameter, and its possible connection with atomistic simulations [357].

In order to simulate crystals the PFC free energy function $F[\rho]$ needs to stabilize long-range order or "wavy features" of $\rho(\mathbf{x}, t)$ inside bulk crystals. This means that in the reciprocal space certain k-wavevector density fluctuations need to be soft. This was achieved in Elder [331] by taking a free energy term of the form:

$$\lambda \int \mathrm{d}\mathbf{x}\rho\left(k_o^2 + \nabla^2\right)^2 \rho/2, \tag{11}$$

and fitting it to the pair correlation function (structure factor) of liquid Ar close to its melting point, measured by neutron diffraction. In two-dimensions a triangular close-packed crystal lattice was thus stabilized. The elastic constants were calculated for the perfect crystal. Then, grain boundaries were created and relaxed and grain boundary energies were evaluated as a function of the misorientation angle, which was shown to follow the Read–Shockley relation [370] with energy cusps (singularities). This suggested the existence of crystallographic dislocations in PFC. Indeed, when simulating epitaxial crystal growth from a liquid dislocations were found to nucleate spontaneously, and then move along slip planes to reduce the elastic strain energy in the film. Crack nucleation and propagation were also demonstrated [331].

The detailed processes of edge dislocation glide, climb and annihilation were examined by PFC in two-dimensions [371]. The energetic behavior of an edge dislocation was found to follow that suggested by the Peierls–Nabarro model [1,232], with an increasing dislocation core width corresponding to a reduced Peierls barrier. However, the dynamics of dislocation motion are not entirely realistic, in the sense that they corresponds to an over-damped system. The inertia effect, which comes from the second order $\ddot{\mathbf{x}}_i$ term in the Newtonian equations of motion, is entirely absent in Berry et al. [371], since the Onsager linear response formalism [361] is first order in time. This difficulty arises because the coarse graining timescale Δt in Eqs. (10a) and (10b) is much larger than the elastodynamic response time of an atomic resolution system, which is t_V. This deficiency was later addressed by Stefanovic et al. [372] for situations where the elastodynamic effects are deemed important, for instance correlated defect propagation where isothermal transition state theory [373] breaks down. Dislocation emission and absorption from grain boundaries, as well as grain rotation and grain boundary migration, have been demonstrated for stressed PFC nanocrystals [374].

To connect with coarser scale continuum descriptions there have been attempts to derive renormalization group reduction [195,375–377] of PFC with adaptive meshing [378], where a density wave (complex amplitude) "envelop function" is used to represent the mostly perfect crystalline regions within each grain. This method has been applied to study grain growth. Stress-driven morphological instabilities such as the Asaro–Tiller–Grinfeld instability of strained films [77,87,311,322–324] has also been studied by PFC [379] at diffusive timescales. Continuum elasticity prediction of the unstable wavelength (leading to island formation) was obtained, within the limit of small misfit stresses.

Efforts to improve the stability and efficiency of PFC simulations are currently underway [380,381]. It should be noted that compared with traditional molecular dynamics simulations, while the temporal scales reached by PFC are superior, the usage of a planewave basis to resolve the atomic density wave at sub-angstrom resolution makes

simulating a large number of atomic sites in three-dimensions quite expensive [382]. Suppose that 20 grid points are required to realistically resolve the atomic density of one vibrational site in one direction – as the Lindemann melting criterion [383] states that a crystal should collapse when the Debye–Waller broadening [362,363] reaches more than ~15% of the nearest neighbor bond length – 8000 grid points are required to satisfactorily represent one atomic site and its relatively narrow density peak in three-dimensions. Suppose that 10^6 solid atoms are simulated, the typical size in present molecular dynamics simulations, it would require 64 GB of memory just to store $\rho(\mathbf{x}, t)$. The usage of a planewave basis in current PFC simulations is predicated by high order gradient operators contained in terms like Eq. (11), which is more efficiently treated in reciprocal space than in real space, similarly to the historical development of prevalent DFT codes for electronic structure calculations. However, the physical meaning of Eq. (11) is less transparent, and good fitting to the liquid structure factor can only be achieved for certain k-ranges and temperatures that may not be representative of solid-state energetics at low temperatures. For the above conceptual and algorithmic reasons it is perhaps advantageous to also develop a completely real space counterpart to PFC, using a Gaussian basis set instead of a planewave basis [384]. A Gaussian-based method under development is called diffusive molecular dynamics (DMD), which is based on a more thorough treatment of the vibrational free energy at the low temperature limit, in contrast to the present PFC formulation, which may be regarded as a high temperature expansion around the liquid–solid coexistence temperature. The mesh-free algorithm of DMD is much closer to traditional atomistic simulations of discrete atoms than continuum field-based simulations. Efforts are also being made to utilize realistic interatomic potentials, such as embedded atom method (EAM) potentials, and the microscopic diffusional mobility database, which is predicated upon local bonding environments [384].

To summarize, the PFC method is a promising technique operating on diffusive timescales and at atomic spatial resolution. It turns the traditional view of fields and particles on its head: most researchers in the mechanics of materials community would regard continuum fields as "larger" than a particle, but a particle is "larger" than the field in PFC. The method has demonstrated great potential in treating defects and deformation, especially coupled diffusional–displacive processes. Significant developments are still needed to turn this promising method into a materials-specific simulation tool.

8. Concluding remarks

Continuum approaches will remain important at the nanoscale and atomic scales. Rather than competing with atomistic simulations, they embrace the discrete atom nature of matter and attempt the best matched-asymptote continuum description, in the spirit of the gradient thermodynamics approach of van der Waals to Cahn. The goal is to achieve particle–field unity out of duality. The following unique features have made the phase field approach a useful means in modeling microstructural evolution, especially when there are complex chemical and structural interactions:

- direct utilization of *ab initio* energetics (rather than through a proxy of fitted interatomic potentials);
- incorporation of thermochemical and diffusive kinetics databases;
- a simplified and parameterized view of complicated processes.

Plasticity and fracture in real materials are often complex as a rule, rather than as an exception. While a certain amount of simplification is desirable, the complexities can only be boiled down to an irreducible set. The phase field approach, incorporating diffusive and displacive degrees of freedom, and carefully calibrated against atomistic simulations for model interatomic potentials, are well suited to treat these chemical and microstructural complexities in an integrated manner.

Acknowledgements

We would like to thank Profs Jin and Wang at Michigan Tech., Dr. Chen Shen at GE Global Research Center and Prof. Dregia and Dr. Ning Zhou at OSU for many useful discussions. We gratefully acknowledge financial support by the National Science Foundation (Grant No. CMMI-0728069) and the Office of Naval Research through the D 3D program (Grant No. N00014-05-1-0504). Y.W. would also like to acknowledge the support of the US Air Force Office of Scientific Research through the Metals Affordability Initiative Program on Durable High Temperature Disks and the STW21 Program on Multi-Materials System with Adaptive Microstructures for Aerospace Applications (Grant No. FA9550-09-1-0014). J.L. would like to acknowledge the support of the US Air Force Office of Scientific Research (Grant No. FA9550-08-1-0325) and Department of Energy (Grant No. DOE-DE-FG02-06ER46330). The simulations cited in some of the examples were performed on supercomputers at the Arctic Region Supercomputing Center and the Ohio Supercomputing Center.

References

[1] Peierls R. Proc Phys Soc London 1940;52:34.
[2] Kroner E. Continuum theory of defects. In: Balian R, editor. Proc Les Houches XXXV. Amsterdam: North-Holland; 1980. p. 282.
[3] Hill R. The mathematical theory of plasticity. Oxford (UK): Clarendon Press; 1950.
[4] Raabe et al. Acta Mater 2010;58:1152.
[5] Mishin et al. Acta Mater 2010;58:1117.
[6] Lepinoux J, Kubin LP. Scripta Metall 1987;21:833.
[7] Gulluoglu AN, Srolovitz DJ, Lesar R, Lomdahl PS. Scripta Metall 1989;23:1347.

[8] Amodeo RJ, Ghoniem NM. Phys Rev B 1990;41:6958.
[9] van der Giessen E, Needleman A. Modell Simul Mater Sci Eng 1995;3:689.
[10] Zbib HM, Rhee M, Hirth JP. Int J Mech Sci 1998;40:113.
[11] Bulatov V, Abraham FF, Kubin L, Devincre B, Yip S. Nature 1998;391:669.
[12] Devincre B, Hoc T, Kubin L. Science 2008;320:1745.
[13] Weygand D, Poignant M, Gumbsch P, Kraft O. Mater Sci Eng A – Struct Mater Prop Microstruct Process 2008;483:188.
[14] Li J, Ngan AHW, Gumbsch P. Acta Mater 2003;51:5711.
[15] Kohn W. Rev Mod Phys 1999;71:1253.
[16] Li J, Liao DY, Yip S. Phys Rev E 1998;57:7259.
[17] Gear CW, Li J, Kevrekidis IG. Phys Lett A 2003;316:190.
[18] Li J, Kevrekidis PG, Gear CW, Kevrekidis LG. SIAM Rev 2007;49:469.
[19] Cai W, Arsenlis A, Weinberger CR, Bulatov VV. J Mech Phys Solids 2006;54:561.
[20] Weinberger CR, Cai W. J Mech Phys Solids 2007;55:2027.
[21] Johnston WG, Gilman JJ. J Appl Phys 1959;30:129.
[22] Walgraef D, Aifantis EC. J Appl Phys 1985;58:688.
[23] Aifantis EC. Int J Plast 1987;3:211.
[24] Fleck NA, Muller GM, Ashby MF, Hutchinson JW. Acta Metall Mater 1994;42:475.
[25] Hahner P, Bay K, Zaiser M. Phys Rev Lett 1998;81:2470.
[26] Arsenlis A, Parks DM. Acta Mater 1999;47:1597.
[27] Gao H, Huang Y, Nix WD, Hutchinson JW. J Mech Phys Solids 1999;47:1239.
[28] Huang Y, Gao H, Nix WD, Hutchinson JW. J Mech Phys Solids 2000;48:99.
[29] Acharya A, Bassani JL. J Mech Phys Solids 2000;48:1565.
[30] Arsenlis A, Parks DM. J Mech Phys Solids 2002;50:1979.
[31] Aifantis EC. Mech Mater 2003;35:259.
[32] Groma I, Csikor FF, Zaiser M. Acta Mater 2003;51:1271.
[33] Arsenlis A, Parks DM, Becker R, Bulatov VV. J Mech Phys Solids 2004;52:1213.
[34] Zaiser M, Hochrainer T. Scripta Mater 2006;54:717.
[35] Gurtin ME, Anand L, Lele SP. J Mech Phys Solids 2007;55:1853.
[36] Dimiduk DM, Uchic MD, Rao SI, Woodward C, Parthasarathy TA. Modell Simul Mater Sci Eng 2007;15:135.
[37] El-Azab A, Zaiser M, Busso EP. Philos Mag 2007;87:1159–446.
[38] Kohlhoff S, Gumbsch P, Fischmeister HF. Philos Mag A – Phys Condens Matter Struct Defects Mech Prop 1991;64:851.
[39] Tadmor EB, Ortiz M, Phillips R. Philos Mag A – Phys Condens Matter Struct Defects Mech Prop 1996;73:1529.
[40] Shenoy VB, Miller R, Tadmor EB, Rodney D, Phillips R, Ortiz M. J Mech Phys Solids 1999;47:611.
[41] Li J, Van Vliet KJ, Zhu T, Yip S, Suresh S. Nature 2002;418:307.
[42] Rudd RE, Broughton JQ. Phys Rev B 2005;72:144104.
[43] Dupuy LM, Tadmor EB, Miller RE, Phillips R. Phys Rev Lett 2005;95:060202.
[44] Tang Z, Zhao H, Li G, Aluru NR. Phys Rev B 2006;74:064110.
[45] Eidel B, Stukowski A. J Mech Phys Solids 2009;57:87.
[46] Ortiz M. J Appl Mech – Trans ASME 1999;66:289.
[47] Onuki A. Phys Rev E 2003;68:061502.
[48] Otsuka K, Ren XB. Intermetallics 1999;7:511.
[49] Otsuka K, Ren X. Prog Mater Sci 2005;50:511.
[50] Wang YU, Jin YM, Cuitino AM, Khachaturyan AG. Acta Mater 2001;49:1847.
[51] Jin YM, Khachaturyan AG. Philos Mag Lett 2001;81:607.
[52] Haataja M, Muller J, Rutenberg AD, Grant M. Phys Rev B 2002;65:165414.
[53] Koslowski M, Cuitino AM, Ortiz M. J Mech Phys Solids 2002;50:2597.
[54] Shen C, Wang Y. Acta Mater 2003;51:2595.
[55] Rodney D, Le Bouar Y, Finel A. Acta Mater 2003;51:17.
[56] Shen C, Wang Y. Acta Mater 2004;52:683.
[57] Hu SY, Li YL, Zheng YX, Chen LQ. Int J Plast 2004;20:403.
[58] Onuki A. J Phys Soc Jpn 1989;58:3065.
[59] Onuki A, Nishimori H. Phys Rev B 1991;43:13649.
[60] Khachaturyan AG, Semennovskaya S, Tsakalakos T. Phys Rev B 1995;52:15909.
[61] Hu SY, Chen LQ. Acta Mater 2001;49:1879.
[62] Wang YU, Jin YM, Khachaturyan AG. J Appl Phys 2002;92:1351.
[63] Wang YU, Jin YM, Khachaturyan AG. Acta Mater 2003;51:4209.
[64] Karma A, Plapp M. Phys Rev Lett 1998;81:4444.
[65] Lu W, Suo Z. Phys Rev B 2002;65:085401.
[66] Lu W, Suo Z. Phys Rev B 2002;65:205418.
[67] Emmerich H. Continuum Mech Thermodyn 2003;15:197.
[68] Wang YU, Jin YMM, Khachaturyan AG. Acta Mater 2004;52:81.
[69] Ratz A, Ribalta A, Voigt A. J Comput Phys 2006;214:187.
[70] Wang YU, Jin YMM, Khachaturyan AG. Philos Mag 2005;85:261.
[71] Mahadevan M, Bradley RM. Phys Rev B 1999;59:11037.
[72] Bhate DN, Kumar A, Bower AF. J Appl Phys 2000;87:1712.
[73] Jin YM, Wang YU, Khachaturyan AG. Appl Phys Lett 2001;79:3071.
[74] Wang YU, Jin YMM, Khachaturyan AG. J Appl Phys 2002;91:6435.
[75] Jin YMM, Wang YU, Khachaturyan AG. Philos Mag 2003;83:1587.
[76] Yu HC, Lu W. Acta Mater 2005;53:1799.
[77] Kassner K, Misbah C. Europhys Lett 1999;46:217.
[78] Aranson IS, Kalatsky VA, Vinokur VM. Phys Rev Lett 2000;85:118.
[79] Karma A, Kessler DA, Levine H. Phys Rev Lett 2001;87:045501.
[80] Eastgate LO, Sethna JP, Rauscher M, Cretegny T, Chen CS, Myers CR. Phys Rev E 2002;65:036117.
[81] Karma A, Lobkovsky AE. Phys Rev Lett 2004;92:245510.
[82] Henry H, Levine H. Phys Rev Lett 2004;93:105504.
[83] Hakim V, Karma A. Phys Rev Lett 2005;95:235501.
[84] Spatschek R, Hartmann M, Brener E, Muller-Krumbhaar H, Kassner K. Phys Rev Lett 2006;96:015502.
[85] Ma XQ, Shi SQ, Woo CH, Chen LQ. Mech Mater 2006;38:3.
[86] Guo XH, Shi SQ, Qiao LJ. J Am Ceram Soc 2007;90:2868.
[87] Spatschek R, Muller-Gugenberger C, Brener E, Nestler B. Phys Rev E Stat Nonlinear Soft Matter Phys 2007;75:066111.
[88] Henry H. Epl 2008;83:16004.
[89] Hakim V, Karma A. J Mech Phys Solids 2009;57:342.
[90] Caginalp G. Arch Ration Mech Anal 1986;92:205.
[91] Penrose O, Fife PC. Phys D 1990;43:44.
[92] Chen LQ, Khachaturyan AG. Acta Metall Mater 1991;39:2533.
[93] Chen LQ, Wang YZ, Khachaturyan AG. Philos Mag Lett 1991;64:241.
[94] Wheeler AA, Boettinger WJ, McFadden GB. Phys Rev A 1992;45:7424.
[95] Wang Y, Chen LQ, Khachaturyan AG. Acta Metall Mater 1993;41:279.
[96] Wang SL, Sekerka RF, Wheeler AA, Murray BT, Coriell SR, Braun RJ, et al. Phys D 1993;69:189.
[97] Kobayashi R. Phys D 1993;63:410.
[98] Warren JA, Boettinger WJ. Acta Metall Mater 1995;43:689.
[99] Pollock TM, Argon AS. Acta Metall Mater 1992;40:1.
[100] Pollock TM, Argon AS. Acta Metall Mater 1994;42:1859.
[101] Kovarik L, Unocic RR, Li J, Mills MJ. JOM 2009;61:42.
[102] Kovarik L, Unocic RR, Li J, Sarosi P, Shen C, Wang Y, et al. Prog Mater Sci 2009;54:839.
[103] Zhou N, Shen C, Mills MJ, Wang Y. Acta Mater 2007;55:5369.
[104] Gaubert A, Finel A, Bouar YL, Boussinot G. Viscoplastic phase field modelling of rafting in Ni base superalloys. In: Jeulin D, Forest S, editors. Continuum models and discrete systems (CMDS 11). Paris: Les Presses de l'Ecole des Mines; 2007. p. 161.
[105] Zhou N, Shen C, Mills MJ, Wang Y. Acta Mater 2008;56:6156.
[106] Zhou N, Shen C, Sarosi PM, Mills MJ, Pollock T, Wang Y. Mater Sci Technol 2009;25:205.
[107] Zhou N, Shen C, Mills MJ, Wang Y. Philos Mag A in press.
[108] Chen LQ. Scripta Metall Mater 1995;32:115.
[109] Kazaryan A, Wang Y, Dregia SA, Patton BR. Phys Rev B 2000;61:14275.
[110] Kobayashi R, Warren JA, Carter WC. Phys D – Nonlinear Phenom 2000;140:141.

[111] Krill CE, Chen LQ. Acta Mater 2002;50:3057.
[112] Kazaryan A, Wang Y, Dregia SA, Patton BR. Acta Mater 2002;50:2491.
[113] Warren JA, Kobayashi R, Lobovsky AE, Carter WC. Acta Mater 2003;51:6035.
[114] Granasy L, Pusztai T, Borzsonyi T, Warren JA, Douglas JF. Nat Mater 2004;3:645.
[115] Ma N, Kazaryan A, Dregia SA, Wang Y. Acta Mater 2004;52:3869.
[116] Tang M, Carter WC, Cannon RM. Phys Rev B 2006;73:024102.
[117] Upmanyu M, Srolovitz DJ, Lobkovsky AE, Warren JA, Carter WC. Acta Mater 2006;54:1707.
[118] Wang Y, Chen LQ, Khachaturyan AG. Modeling of dynamical evolution of micro/mesoscopic morphological patterns in coherent phase transformations. In: Kirchner HO, Kubin KP, Pontikis V, editors. Computer simulation in materials science – nano/meso/macroscopic space and time scales. Dordrecht: Kluwer; 1996. p. 25.
[119] Zhu JZ, Liu ZK, Vaithyanathan V, Chen LQ. Scripta Mater 2002;46:401.
[120] Thornton K, Agren J, Voorhees PW. Acta Mater 2003;51:5675.
[121] Thornton K, Akaiwa N, Voorhees PW. Acta Mater 2004;52:1353.
[122] Fan D, Chen SP, Chen LQ. J Mater Res 1999;14:1113.
[123] Hu SY, Chen LQ. Acta Mater 2001;49:463.
[124] Cha PR, Kim SG, Yeon DH, Yoon JK. Acta Mater 2002;50:3817.
[125] Ma N, Dregia SA, Wang Y. Acta Mater 2003;51:3687.
[126] Ma N, Shen C, Dregia SA, Wang Y. Metall Mater Trans A – Phys Metall Mater Sci 2006;37A:1773.
[127] Gronhagen K, Agren J. Acta Mater 2007;55:955.
[128] Kim SG, Park YB. Acta Mater 2008;56:3739.
[129] Suresh S, Li J. Nature 2008;456:716.
[130] Sundman B, Jansson B, Andersson JO. Calphad – Comput Coupl Phase Diagrams Thermochem 1985;9:153.
[131] Chen SL, Daniel S, Zhang F, Chang YA, Yan XY, Xie FY, et al. Calphad – Comput Coupl Phase Diagrams Thermochem 2002;26:175.
[132] Bale C, Chartrand P, Degterov SA, Eriksson G, Hack K, Ben Mahfoud R, et al. Calphad – Comput Coupl Phase Diagrams Thermochem 2002;26:189.
[133] Davies RH, Dinsdale AT, Gisby JA, Robinson JAJ, Martin SM. Calphad – Comput Coupl Phase Diagrams Thermochem 2002;26:229.
[134] Andersson JO, Helander T, Hoglund LH, Shi PF, Sundman B. Calphad – Comput Coupl Phase Diagrams Thermochem 2002;26:273.
[135] Turchi PEA, Abrikosov IA, Burton B, Fries SG, Grimvalle G, Kaufman L, et al. Calphad – Comput Coupl Phase Diagrams Thermochem 2007;31:4.
[136] Grafe U, Bottger B, Tiaden J, Fries SG. Scripta Mater 2000;42:1179.
[137] Cha PR, Yeon DH, Yoon JK. Acta Mater 2001;49:3295.
[138] Yeon DH, Cha PR, Yoon JK. Scripta Mater 2001;45:661.
[139] Loginova I, Odqvist J, Amberg G, Agren J. Acta Mater 2003;51:1327.
[140] Qin RS, Wallach ER. Acta Mater 2003;51:6199.
[141] Chen Q, Ma N, Wu KS, Wang YZ. Scripta Mater 2004;50:471.
[142] Wu K, Chang YA, Wang Y. Scripta Mater 2004;50:1145.
[143] Wen YH, Wang B, Simmons JP, Wang Y. Acta Mater 2006;54:2087.
[144] Eiken J, Bottger B, Steinbach I. Phys Rev E 2006;73:066122.
[145] Fries SG, Boettger B, Eiken J, Steinbach I. Int J Mater Res 2009;100:128.
[146] Hohenberg PC, Halperin BI. Rev Mod Phys 1977;49:435.
[147] Gunton JD, Miguel MS, Sahni PS. The dynamics of first-order phase transitions. In: Domb C, Lebowitz JL, editors. Phase transitions and critical phenomena, vol. 8. New York: Academic Press; 1983.
[148] Elder KR. Comput Phys 1993;7:27.
[149] Wang YZ, Chen LQ. Simulation of microstructural evolution using the field method. In: Kaufmann EN, editor. Methods in materials research. New York: Wiley; 2000. p. 2a.3.1.
[150] Karma A. Phase field methods. In: Buschow KHJ, Cahn RW, Flemings MC, Ilschner B, Kramer EJ, Mahajian S, editors. Encyclopedia of materials: science and technology, vol. 7. Oxford (UK): Elsevier; 2001. p. 873.
[151] Boettinger WJ, Warren JA, Beckermann C, Karma A. Ann Rev Mater Res 2002;32:163.
[152] Chen LQ. Ann Rev Mater Res 2002;32:113.
[153] Emmerich H. The diffuse interface approach in materials science. Thermodynamic concepts and applications of phase-field models. Berlin: Springer; 2003.
[154] Shen C, Wang Y. Coherent precipitation – phase field method. In: Yip S, editor. Handbook of materials modeling, vol. B: Models. Berlin: Springer; 2005. p. 117.
[155] Emmerich H, Siquieri R. Selected problems of phase-field modeling in materials science. In: Gottstein G, editor. Integral materials modeling: towards physics-based through-process models. Weinheim, Germany: Weinheim; 2007.
[156] Emmerich H. Adv Phys 2008;57:1.
[157] Steinbach I. Modell Simul Mater Sci Eng 2009;17:073001.
[158] Trivedi R. Theory of capillarity. In: Aaronson HI, editor. Lectures on the theory of phase transformations. Warrendale (PA): TMS; 1999. p. 135.
[159] Sutton AP, Balluffi RW. Interfaces in crystalline materials. Oxford (UK): Clarendon Press; 1995.
[160] Gibbs JW. The scientific papers of J. Willard Gibbs. Whitefish (MT): Kessinger Publishing; 2007.
[161] Lupis CHP. Chemical thermodynamics of materials. New York: North-Holland; 1983.
[162] van der Waals JD. Konink. Akad. Weten. Amsterdam (Sect. 1) 1893;1:56.
[163] Landau L, Lifshitz E. Phys Zeit Sowjetunion 1935;8:153.
[164] Cahn JW, Hilliard JE. J Chem Phys 1958;28:258.
[165] Hillert M. A theory of nucleation of solid metallic solutions. Sc.D. thesis. Cambridge (MA): Massachusetts Institute of Technology; 1956.
[166] Lee YW, Aaronson HI. Acta Metall 1980;28:539.
[167] Langer JS. Ann Phys 1969;54:258.
[168] Langer JS. Ann Phys 1971;65:53.
[169] Elder KR, Provatas N, Berry J, Stefanovic P, Grant M. Phys Rev B 2007;75:064107.
[170] Cahn JW, Hilliard JE. J Chem Phys 1959;31:688.
[171] Mullins WW. In: Carter WC, Johnson WC, editors. The selected works of John W. Cahn. Warrendale (PA): TMS; 1998. p. 25.
[172] Hirth JP. Metall Trans A 1985;16:2085.
[173] Vitek V. Philos Mag 1968;18:773.
[174] Kaxiras E, Duesbery MS. Phys Rev Lett 1993;70:3752.
[175] Zimmerman JA, Gao HJ, Abraham FF. Modell Simul Mater Sci Eng 2000;8:103.
[176] Ogata S, Li J, Yip S. Science 2002;298:807.
[177] Dregia SA, Wynblatt P, Bauer CL. Mat Res Soc Symp Proc 1987;94:111.
[178] Dugdale DS. J Mech Phys Solids 1960;8:100.
[179] Barenblatt GI. Adv Appl Mech 1962;7:55.
[180] Aifantis EC. Int J Eng Sci 1992;30:1279.
[181] Xu XP, Needleman A. J Mech Phys Solids 1994;42:1397.
[182] Camacho GT, Ortiz M. Int J Solids Struct 1996;33:2899.
[183] Gao HJ, Klein P. J Mech Phys Solids 1998;46:187.
[184] Ortiz M, Pandolfi A. Int J Numer Methods Eng 1999;44:1267.
[185] Wells GN, Sluys LJ. Int J Numer Methods Eng 2001;50:2667.
[186] Moes N, Belytschko T. Eng Fract Mech 2002;69:813.
[187] Bloch F. Z Phys 1932;74:295.
[188] Cahn JW. Acta Metall 1961;9:795.
[189] Allen SM, Cahn JW. Acta Metall 1979;27:1085.
[190] Khachaturyan AG. Soviet Phys Solid State, Ussr 1968;9:2040.
[191] Wang Y. Theoretical characterization and modeling of microstructure development during coherent phase transformations in metals and ceramics. Ph.D. thesis. Rutgers University; 1995.
[192] Harrowell PR, Oxtoby DW. J Chem Phys 1987;86:2932.
[193] Khachaturyan AG. Philos Mag A – Phys Condens Matter Struct Defect Mech Prop 1996;74:3.

[194] Venkitachalam MK, Chen LQ, Khachaturyan AG, Messing GL. Mater Sci Eng A 1997;238:94.
[195] Goldenfeld N, Athreya BP, Dantzig JA. Phys Rev E 2005;72:020601.
[196] Yeon DH, Huang Z-F, Elder KR, Thornton K. Philos Mag in press.
[197] Hoyt JJ, Asta M, Karma A. Phys Rev Lett 2001;86:5530.
[198] Foiles SM, Hoyt JJ. Acta Mater 2006;54:3351.
[199] Ono S. Memoirs of the faculty of engineering. Kyushu University, vol. 10; 1947. p. 195.
[200] Hillert M. Acta Metall 1961;9:525.
[201] Wang YZ, Khachaturyan AG. Mater Sci Eng A 2006;438:55.
[202] Shen C, Li J, Wang YZ. Metall Mater Trans A 2008;39:976.
[203] Ogata S, Li J, Yip S. Phys Rev B 2005;71:224102.
[204] Trinkle DR, Hennig RG, Srinivasan SG, Hatch DM, Jones MD, Stokes HT, et al. Phys Rev Lett 2003;91:025701.
[205] Caspersen KJ, Carter EA. PNAS 2005;102:6738.
[206] Li J, Liao DY, Yip S, Najafabadi R, Ecker L. J Appl Phys 2003;93:9072.
[207] Wang YU, Jin YMM, Khachaturyan AG. Dislocation dynamics – phase field. In: Yip S, editor. Handbook of materials modeling, vol. B: Models. Berlin: Springer; 2005. p. 2287.
[208] Karma A, Rappel W-J. Phys Rev E 1998;57:4323.
[209] Karma A, Rappel W-J. Phys Rev E 1996;53:R3017.
[210] Almgren RF. SIAM J Appl Math 1999;59:2086.
[211] McFadden GB, Wheeler AA, Anderson DM. Phys D 2000;144:154.
[212] Elder KR, Grant M, Provatas N, Kosterlitz JM. Phys Rev E 2001;64:021604.
[213] Shen C, Chen Q, Wen YH, Simmons JP, Wang Y. Scripta Mater 2004;50:1023.
[214] Shen C, Chen Q, Wen YH, Simmons JP, Wang Y. Scripta Mater 2004;50:1029.
[215] Tiaden J, Nestler B, Diepers HJ, Steinbach I. Phys D 1998;115:73.
[216] Kim SG, Kim WT, Suzuki T. Phys Rev E 1999;60:7186.
[217] Provatas N, Goldenfeld N, Dantzig J. Phys Rev Lett 1998;80:3308.
[218] Feng WM, Yu P, Hu SY, Liu ZK, Du Q, Chen LQ. J Comput Phys 2006;220:498.
[219] Braun RJ, Murray BT. J Cryst Growth 1997;174:41.
[220] Lan CW, Hsu CM, Liu CC, Chang YC. Phys Rev E 2002;65:061601.
[221] Provatas N, Greenwood M, Athreya B, Goldenfeld N, Dantzig J. Int J Mod Phys B 2005;19:4525.
[222] Stogner RH, Carey GF, Murray BT. Int J Numer Methods Eng 2008;76:636.
[223] Gruber J, Ma N, Rollett AD, Rohrer GS. Modell Simul Mater Sci Eng 2006;14:1189.
[224] Vedantam S, Patnaik BS. Phys Rev E 2006;73:016703.
[225] Shen C, Li J, Mills MJ, Wang Y. Modeling shearing of γ' in Ni-based superalloys. In: Gottstein G, editor. Integral materials modeling: towards physics-based through-process models. Weinheim, Germany: Wiley-VCH Verlag; 2007. p. 243.
[226] Khachaturyan AG. Sov Phys Solid State 1967;8:2163.
[227] Khachaturyan AG, Shatalov GA. Sov Phys Solid State 1969;11:118.
[228] Khachaturyan AG. Theory of structural transformations in solids. New York: John Wiley & Sons; 1983.
[229] Eshelby JD. Proc R Soc London, Ser A 1957;241:376.
[230] Eshelby JD. Proc R Soc London, Ser A 1959;252:561.
[231] Chen LQ, Wang YZ, Khachaturyan AG. Philos Mag Lett 1992;65:15.
[232] Nabarro FRN. Proc Phys Soc London 1947;59:256.
[233] Bullough R, Tewary VK. Lattice theories of dislocations. In: Nabarro FRN, editor. Dislocations in solids, vol. 2. Amsterdam: Elsevier; 1979. p. 1.
[234] Bulatov VV, Kaxiras E. Phys Rev Lett 1997;78:4221.
[235] Lu G, Zhang Q, Kioussis N, Kaxiras E. Phys Rev Lett 2001;8709:095501.
[236] Lu G, Bulatov VV, Kioussis N. Int J Plast 2004;20:447.
[237] Wang Y, Khachaturyan AG. Acta Mater 1997;45:759.
[238] Joos B, Duesbery MS. Phys Rev Lett 1997;78:266.
[239] Schoeck G. Comput Mater Sci 2001;21:124.
[240] Joos B, Zhou J. Philos Mag A – Phys Condens Matter Struct Defects Mech Prop 2001;81:1329.
[241] Shen Y, Cheng X. Scripta Mater 2009;61:457.
[242] Shen Y, Li Y, Li ZH, Wan HB, Nie PL. Scripta Mater 2009;60:901.
[243] Kresse G, Furthmuller J. Phys Rev B 1996;54:11169.
[244] Wang SF. Phys Rev B 2002;65:094111.
[245] Foreman AJ, Jaswon MA, Wood JK. Proc Phys Soc London, Sect A 1951;64:156.
[246] Shen C, Li J, Wang Y.
[247] Rice JR. J Mech Phys Solids 1992;40:239.
[248] Rice JR, Beltz GE. J Mech Phys Solids 1994;42:333.
[249] Rice JR, Thomson R. Philos Mag 1974;29:73.
[250] Xu G, Argon AS, Oritz M. Philos Mag A – Phys Condens Matter Struct Defects Mech Prop 1997;75:341.
[251] Xu G, Argon AS, Ortiz M. Philos Mag A – Phys Condens Matter Struct Defects Mech Prop 1995;72:415.
[252] Tadmor EB, Hai S. J Mech Phys Solids 2003;51:765.
[253] Wang YU, Jin YMM, Khachaturyan AG. Acta Mater 2004;52:1039.
[254] Li DY, Chen LQ. Scripta Mater 1997;37:1271.
[255] Schoeck G, Kohlhammer S, Fähnle M. Philos Mag Lett 1999;79:849.
[256] Lu G, Kioussis N, Bulatov VV, Kaxiras E. Phys Rev B 2000;62:3099.
[257] Amelinckx S. The direct observation of dislocations. In: Seitz F, Turnbull D, editors. Solid state physics. vol. 6, suppl. 6. New York: Academic Press; 1964.
[258] Unocic RR, Kovarik L, Shen C, Sarosi PM, Wang Y, Li J, et al. Deformation mechanisms in Ni-base disk superalloys at higher temperatures. In: Reed RC, Green KA, Caron P, Gabb TP, Fahrmann MG, Huron ES, et al., editors. Superalloys 08. Warrendale (PA): TMS; 2008. p. 377.
[259] Hennig RG, Trinkle DR, Bouchet J, Srinivasan SG, Albers RC, Wilkins JW. Nat Mater 2005;4:129.
[260] Hatcher N, Kontsevoi OY, Freeman AJ. Phys Rev B 2009;79:020202.
[261] Olson GB. Mater Sci Eng A – Struct Mater Prop Microstruct Process 1999;273:11.
[262] Friak M, Sob M, Vitek V. Phys Rev B 2001;63:052405.
[263] Bernstein N, Tadmor EB. Phys Rev B 2004;69:094116.
[264] Warner DH, Curtin WA, Qu S. Nat Mater 2007;6:876.
[265] Chen MW, Ma E, Hemker KJ, Sheng HW, Wang YM, Cheng XM. Science 2003;300:1275.
[266] Liao XZ, Zhou F, Lavernia EJ, Srinivasan SG, Baskes MI, He DW, et al. Appl Phys Lett 2003;83:632.
[267] Kaufmann HJ, Luft A, Schulze D. Cryst Res Technol 1984;19:357.
[268] Pirouz P. Scripta Metall 1987;21:1463.
[269] Lagerlof KPD, Castaing J, Pirouz P, Heuer AH. Philos Mag A 2002;82:2841.
[270] Landau LD, Lifshitz EM. Statistical physics. New York: Pergamon Press; 1980.
[271] Toledano P, Dmitriev V. Reconstructive phase transformations in crystals and quasicrystals. Singapore: World Scientific; 1996.
[272] Cahn JW. Acta Metall 1977;25:721.
[273] Bruinsma R, Zangwill A. J Phys 1986;47:2055.
[274] Olson GB, Cohen M. J Phys Colloq 1982;43:75.
[275] Beauchamp P, Villain JP. J Phys 1983;44:1117.
[276] Olson GB, Roitburd AL. Martensitic nucleation. In: Olson GB, Owen WS, editors. Martensite. Materials Park (OH): ASM International; 1992. p. 149.
[277] Chu FM, Pope DP. Mater Sci Eng A 1993;170:39.
[278] Hazzledine PM, Pirouz P. Scr Metall Mater 1993;28:1277.
[279] Kumar KS, Hazzledine PM. Intermetallics 2004;12:763.
[280] Khachaturyan AG, Suris RA. Sov Phys Cryst 1968;13:63.
[281] Roitburd AL, Khachatu AG, Plaksina TS. Sov Phys Solid State 1969;10:1684.
[282] Legoues FK, Aaronson HI, Lee YW. Acta Metall 1984;32:1845.
[283] Haezebrouck DM. Nucleation and growth of a single martensitic particle. Sc.D. thesis. Cambridge (MA): Massachusetts Institute of Technology; 1987.
[284] Rundle JB, Klein W. Phys Rev Lett 1989;63:171.
[285] Roitburd AL. Mater Sci Eng A 1990;127:229.

[286] Poduri R, Chen LQ. Acta Mater 1996;44:4253.
[287] Roy A, Rickman JM, Gunton JD, Elder KR. Phys Rev E 1998;57:2610.
[288] Reid ACE, Olson GB, Moran B. Phase Trans 1999;69:309.
[289] Chu YA, Moran B, Olson GB. Metall Mater Trans A 2000;31A:1321.
[290] Granasy L, Pusztai T, Borzsonyi T, Toth G, Tegze G, Warren JA, et al. J Mater Res 2006;21:309.
[291] Granasy L, Pusztai T, Saylor D, Warren JA. Phys Rev Lett 2007;98:035703.
[292] Zhang W, Jin YM, Khachaturyan AG. Acta Mater 2007;55:565.
[293] Moran B, Chu YA, Olson GB. Int J Solids Struct 1996;33:1903.
[294] Gránásy L, Börzsönyi T, Pusztai T. Phys Rev Lett 2003;88:206105.
[295] Gagne CJ, Gould H, Klein W, Lookman T, Saxena A. Phys Rev Lett 2005;95:095701.
[296] Khachaturyan AG, Wang Y, Wang HY. Mater Sci Forum 1994;155–156:345.
[297] Wang YZ, Wang HY, Chen LQ, Khachaturyan AG. J Am Ceram Soc 1995;78:657.
[298] Zhang L, Chen LQ, Du Q. Phys Rev Lett 2007;98:265703.
[299] Zhang L, Chen LQ, Du Q. Acta Mater 2008;56:3568.
[300] Zhu T, Li J, Samanta A, Kim HG, Suresh S. PNAS 2007;104:3031.
[301] Henkelman G, Jonsson H. J Chem Phys 2000;113:9978.
[302] Anderson TL. Fracture mechanics: fundamentals and applications. Boca Raton (FL): CRC Press; 2004.
[303] Ogata S, Li J, Hirosaki N, Shibutani Y, Yip S. Phys Rev B 2004;70:104104.
[304] Hutchinson JW. J Mech Phys Solids 1968;16:13.
[305] Rice JR, Rosengren GF. J Mech Phys Solids 1968;16:1.
[306] Celarie F, Prades S, Bonamy D, Ferrero L, Bouchaud E, Guillot C, et al. Phys Rev Lett 2003;90:075504.
[307] Shan ZW, Li J, Cheng YQ, Minor AM, Asif SAS, Warren OL, et al. Phys Rev B 2008;77:155419.
[308] Rose JH, Ferrante J, Smith JR. Phys Rev Lett 1981;47:675.
[309] Zhu T, Li J, Yip S. Phys Rev Lett 2004;93:205504.
[310] Zhu T, Li J, Yip S. Proc R Soc A – Mathe Phys Eng Sci 2006;462:1741.
[311] Yeon DH, Cha PR, Grant M. Acta Mater 2006;54:1623.
[312] Gugenberger C, Spatschek R, Kassner K. Phys Rev E 2008;78:016703.
[313] Freund LB. Dynamic fracture mechanics. Cambridge: Cambridge University Press; 1990.
[314] Song YC, Soh AK, Ni Y. J Phys D – Appl Phys 2007;40:1175.
[315] Wang J, Zhang TY. Acta Mater 2007;55:2465.
[316] Christian JW. The theory of transformations in metals and alloys. Amsterdam: Elsevier; 2002.
[317] Frost HJ, Ashby MF. Deformation-mechanism maps. New York: Pergamon Press; 1982.
[318] Herring C. J Appl Phys 1950;21:437.
[319] Coble RL. J Appl Phys 1963;34:1679.
[320] Weertman J. J Appl Phys 1957;28:362.
[321] Swinkels FB, Ashby MF. Acta Metall 1981;29:259.
[322] Asaro RJ, Tiller WA. Metall Trans 1972;3:1789.
[323] Grinfeld MA. Sov Phys Dokl 1986;31:831.
[324] Srolovitz DJ. Acta Metall 1989;37:621.
[325] Trinkle DR, Woodward C. Science 2005;310:1665.
[326] Curtin WA, Olmsted DL, Hector LG. Nat Mater 2006;5:875.
[327] Hirth JP. Metall Trans A – Phys Metall Mater Sci 1980;11:861.
[328] Birnbaum HK, Sofronis P. Mater Sci Eng A – Struct Mater Prop Microstruct Process 1994;176:191.
[329] Fahrmann M, Hermann W, Fahrmann E, Boegli A, Pollock TM, Sockel HG. Mater Sci Eng A – Struct Mater Prop Microstruct Process 1999;260:212.
[330] Elder KR, Katakowski M, Haataja M, Grant M. Phys Rev Lett 2002;88:245701.
[331] Elder KR, Grant M. Phys Rev E 2004;70:051605.
[332] Khachaturyan AG. Sov Phys – Solid State 1963;5:16.
[333] Khachaturyan AG. Sov Phys – Solid State 1963;5:548.
[334] Khachaturyan AG. Prog Mater Sci 1978;22:1.
[335] Jin YMM, Khachaturyan AG. J Appl Phys 2006;100:013519.
[336] Hansen J-P, McDonald IR. Theory of simple liquids. New York: Academic Press; 2006.
[337] Henderson D, editor. Fundamentals of inhomogeneous fluids. Boca Raton (FL): CRC Press; 1992.
[338] Mermin ND. Phys Rev 1965;137:1441.
[339] Morita T, Hiroike K. Prog Theor Phys 1961;25:537.
[340] Dedominicis C. J Math Phys 1962;3:983.
[341] Stillinger FH, Buff FP. J Chem Phys 1962;37:1.
[342] Lebowitz JL, Percus JK. J Math Phys 1963;4:116.
[343] Ebner C, Saam WF, Stroud D. Phys Rev A 1976;14:2264.
[344] Evans R. Adv Phys 1979;28:143.
[345] Ebner C, Krishnamurthy HR, Pandit R. Phys Rev A 1991;43:4355.
[346] Oxtoby DW. Ann Rev Mater Res 2002;32:39.
[347] Rowlinson JS, Widom B. Molecular theory of capillarity. Oxford (UK): Clarendon Press; 1982.
[348] Kirkwood JG, Monroe E. J Chem Phys 1940;8:845.
[349] Kirkwood JG, Monroe E. J Chem Phys 1941;9:514.
[350] Ramakrishnan TV, Yussouff M. Phys Rev B 1979;19:2775.
[351] Haymet ADJ, Oxtoby DW. J Chem Phys 1981;74:2559.
[352] Oxtoby DW, Haymet ADJ. J Chem Phys 1982;76:6262.
[353] Haymet ADJ, Oxtoby DW. J Chem Phys 1986;84:1769.
[354] Haymet ADJ. Annu Rev Phys Chem 1987;38:89.
[355] Curtin WA, Ashcroft NW. Phys Rev A 1985;32:2909.
[356] Curtin WA, Ashcroft NW. Phys Rev Lett 1986;56:2775.
[357] Tupper PF, Grant M. Epl 2008;81:40007.
[358] Eapen J, Li J, Yip S. Phys Rev E 2005;72:056712.
[359] Witten TA, Pincus PA. Structured fluids: polymers, colloids, surfactants. Oxford: Oxford University Press; 2004.
[360] Larche FC, Cahn JW. Acta Metall 1985;33:331.
[361] Balluffi RW, Allen SM, Carter WC. Kinetics of materials. New York: Wiley; 2005.
[362] Debye P. Ann Phys 1913;43:49.
[363] Waller I. Z Phys Hadrons Nucl 1923;17:398.
[364] Budrovic Z, Van Swygenhoven H, Derlet PM, Van Petegem S, Schmitt B. Science 2004;304:273.
[365] Gianola DS, Van Petegem S, Legros M, Brandstetter S, Van Swygenhoven H, Hemker KJ. Acta Mater 2006;54:2253.
[366] Majaniemi S, Grant M. Phys Rev B 2007;75:054301.
[367] Majaniemi S, Nonomura M, Grant M. Eur Phys J B 2008;66:329.
[368] Runge E, Gross EKU. Phys Rev Lett 1984;52:997.
[369] Kim JH, Garofalini SH. Phys Rev B 2008;78:144109.
[370] Read WT, Shockley W. Phys Rev 1950;78:275.
[371] Berry J, Grant M, Elder KR. Phys Rev E 2006;73:031609.
[372] Stefanovic P, Haataja M, Provatas N. Phys Rev Lett 2006;96:225504.
[373] Li J. MRS Bull 2007;32:151.
[374] Hirouchi T, Takaki T, Tomita Y. Comput Mater Sci 2009;44:1192.
[375] Athreya BP, Goldenfeld N, Dantzig JA. Phys Rev E 2006;74:011601.
[376] Shiwa Y. Phys Rev E 2009;79:013601.
[377] Goldenfeld N, Athreya BP, Dantzig JA. Phys Rev E 2009;79:013602.
[378] Athreya BP, Goldenfeld N, Dantzig JA, Greenwood M, Provatas N. Phys Rev E 2007;76:056706.
[379] Huang ZF, Elder KR. Phys Rev Lett 2008;101:158701.
[380] Cheng M, Warren JA. J Comput Phys 2008;227:6241.
[381] Tegze G, Bansel G, Toth GI, Pusztai T, Fan ZY, Granasy L. J Comput Phys 2009;228:1612.
[382] Berry J, Elder KR, Grant M. Phys Rev E 2008;77:061506.
[383] Lindemann FA. Phys Z 1910;11:609.
[384] Cox WT, Lenosky TJ, Bitzek E, Sarkar S, Wang Y, Li J. in preparation.